HHS Public Access

Author manuscript

Cell Rep. Author manuscript; available in PMC 2024 January 25.

Published in final edited form as:

Cell Rep. 2023 December 26; 42(12): 113486. doi:10.1016/j.celrep.2023.113486.

p120 RasGAP and ZO-2 are essential for Hippo signaling and tumor-suppressor function mediated by p190A RhoGAP

Hanyue Ouyang[1,2,5], **Shuang Wu**[3,5], **Wangji Li**[1], **Michael J. Grey**[1,4], **Wenchao Wu**[2], **Steen H. Hansen**[1,6,*]

[1]GI Cell Biology Laboratory, Boston Children's Hospital, Department of Pediatrics, Harvard Medical School, Boston, MA 02115, USA

[2]State Key Laboratory of Oncology in South China, Guangdong Provincial Clinical Research Center for Cancer, Sun Yat-sen University Cancer Center, Collaborative Innovation Center for Cancer Medicine, Guangzhou 510060, P.R. China

[3]Department of Radiation Oncology, The First Affiliated Hospital, Sun Yat-sen University, Guangzhou, P.R. China

[4]Present address: Division of Gastroenterology, Beth Israel Deaconess Medical Center, Boston, MA, USA

[5]These authors contributed equally

[6]Lead contact

SUMMARY

ARHGAP35, which encodes p190A RhoGAP (p190A), is a major cancer gene. p190A is a tumor suppressor that activates the Hippo pathway. p190A was originally cloned via direct binding to p120 RasGAP (RasGAP). Here, we determine that interaction of p190A with the tight-junction-associated protein ZO-2 is dependent on RasGAP. We establish that both RasGAP and ZO-2 are necessary for p190A to activate large tumor-suppressor (LATS) kinases, elicit mesenchymal-to-epithelial transition, promote contact inhibition of cell proliferation, and suppress tumorigenesis. Moreover, RasGAP and ZO-2 are required for transcriptional modulation by p190A. Finally, we demonstrate that low *ARHGAP35* expression is associated with shorter survival in patients with high, but not low, transcript levels of *TJP2* encoding ZO-2. Hence, we define a tumor-suppressor interactome of p190A that includes ZO-2, an established constituent of the Hippo pathway, and RasGAP, which, despite strong association with Ras signaling, is essential for p190A to activate LATS kinases.

*Correspondence: steen.hansen@childrens.harvard.edu.

AUTHOR CONTRIBUTIONS

Conceptualization, H.O. and S.H.H; methodology, H.O., M.J.G., and S.H.H.; investigation, H.O., S.W., W.L., M.J.G., W.W., and S.H.H.; formal analysis, H.O. and S.H.H; manuscript writing and editing, H.O. and S.H.H.; funding acquisition, S.W. and S.H.H.; resources, W.W. and S.H.H.; project supervision, S.H.H. All authors approved the final version of the manuscript.

SUPPLEMENTAL INFORMATION

Supplemental information can be found online at https://doi.org/10.1016/j.celrep.2023.113486.

DECLARATION OF INTERESTS

The authors declare no competing interests.

Graphical Abstract

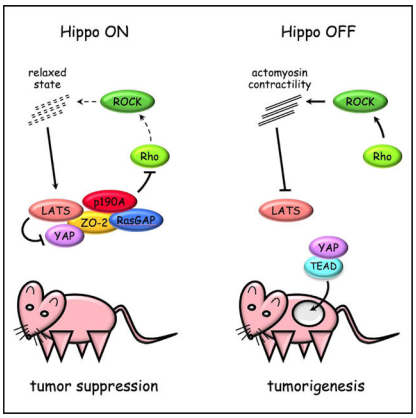

In brief

In this work, Ouyang et al. define interactions of p190A with p120 RasGAP and the tight-junction protein ZO-2 that are necessary for p190A to activate the Hippo pathway, modulate gene transcription, elicit mesenchymal-to-epithelial transition, promote contact inhibition of cell proliferation, and suppress tumorigenesis in a xenograft mouse model.

INTRODUCTION

Major genome-wide association studies (GWASs) published almost a decade ago identified *ARHGAP35* as one of the 30–40 most significantly mutated genes in tumor samples.[1,2] At that time, it was further determined that the region on chromosome 19, where the *ARHGAP35* gene is located, ranks among the most frequently lost in cancer.[3] Since then, there has beena steady trickle of additional GWASs associating *ARHGAP35* alterations with human cancer.[4–14] However, this body of work has been unable to assign a role for *ARHGAP35* in cancer beyond noting that the spectrum of alterations is suggestive of a tumor-suppressor function. *ARHGAP35* encodes p190A RhoGAP (p190A), an enzyme that promotes guanosine triphosphate (GTP) hydrolysis on Rho and Rac GTPases.[15,16] However, p190A is a large and complex protein with a GTPase domain, four FF motifs, two pseudo-GTPase-activating protein (GAP) domains, and an active GAP domain, in addition to sequences of unknown function. These domains modulate GAP activity but also exert scaffolding functions, as exemplified by the direct binding of Rnd proteins and sequestration of the transcription factor TFII-I.[17,18]

Rooted in GWAS data, we have relied on unbiased approaches to elucidate a role for p190A in epithelial oncogenesis because *ARHGAP35* alterations are predominantly found in carcinomas (gdc.cancer.gov). Our initial efforts have led to the discovery that p190A promotes contact inhibition of cell proliferation (CIP) via mechanotransduction and the Hippo pathway to repress the activity of the proto-oncogenic transcriptional co-activator YAP.[19] Moreover, we determined that restoring p190A expression in cancer cells with defined *ARHGAP35* alteration induces expression of *CDH1* encoding E-cadherin to establish a feedforward loop that activates large tumor-suppressor (LATS) kinases and

promotes mesenchymal-to-epithelial transition (MET). We furthermore provided direct demonstration of p190A functioning as a tumor suppressor *in vivo* and determined that recurrent *ARHGAP35* mutations in human tumor samples exhibit loss of function.[20]

A role for p190A in promoting GTP hydrolysis of Rho proteins is well established.[21] In contrast, it is unclear how p190A might activate the Hippo pathway. In this work, we have used mass spectrometry to identify p190A-interacting proteins that may account for the capacity of p190A to activate LATS kinases. The most frequently interacting proteins identified were RasGAP and ZO-1/2 encoded by *RASA1* and *TJP1/2*, respectively. Here, we determine that p190A binds ZO-1/2 in a RasGAP-dependent manner and that interactions with RasGAP and ZO-2 are obligatory for p190A to activate LATS kinases, elicit MET, induce CIP, and suppress tumorigenesis. Moreover, we establish that RasGAP and ZO-2 play essential roles in transcriptional alterations elicited by expression of p190A. Finally, we demonstrate that expression of *ARHGAP35* in human tumors correlates with Hippo signaling and that the impact of *ARHGAP35* alteration on survival of patients with lung adenocarcinoma (LUAD) is influenced by *TJP1* and *TJP2* transcript levels. Collectively, these findings define a tumor-suppressor interactome of p190A consisting of RasGAP,[22] a negative regulator of Ras signaling, and ZO-2, a tight-junction constituent and modulator of YAP/TAZ transcriptional co-activators.[23]

RESULTS

Direct binding to RasGAP is required for p190A to activate LATS kinases, elicit MET, and promote CIP

Our published studies have established a pivotal role for p190A in activation of LATS kinases.[19,20] However, the mechanism by which p190A exerts this function is not well understood. In this work, we tested the hypothesis that p190A might bind to upstream constituents of the Hippo pathway. To this end, we exploited the fact that expression of Myc-tagged p190A in non-small cell lung cancer (NSCLC) NCI-H661 (H661) cells, which harbor defined *ARHGAP35* loss-of-function alterations, activates LATS kinases to suppress oncogenic capacities.[20] Hence, in these H661-p190A cells, we have established that the link between p190A and the Hippo pathway is intact. We therefore immunoprecipitated Myc-p190A with anti-Myc 9E10 antibody from control and H661-p190A cells and subjected the samples to mass spectrometry analysis. Two classes of co-immunoprecipitating proteins were identified more frequently than others (Figures S1A and S1B). The first was RasGAP, which was reassuring, as p190A initially was cloned via its direct binding to RasGAP[15,24] (Figure S1C). The second was the tight-junction-associated zonula occludens proteins ZO-1 and ZO-2.[25,26]

We initially focused on the interaction with RasGAP, which is well established to augment the RhoGAP activity of p190A and promote directional motility.[27,28] However, in cancer biology, RasGAP is primarily implicated in Ras signaling and is invariably assigned this role in GWASs.[22] We considered the intriguing possibility that RasGAP might impact the Hippo pathway via p190A. To this end, we knocked out *RASA1* encoding RasGAP from H661 cells using CRISPR-Cas9 technology (Figure S1D). Strikingly, p190A was unable to activate LATS kinases in cells depleted of RasGAP (Figures 1A and 1B). Equally, the

capacity of p190A to induce CIP, which is mediated by the Hippo pathway, was significantly perturbed in H661-p190A *RASA1*-knockout (KO) cells (Figures 1A and 1B). Next, we tested whether direct interaction between RasGAP and p190A is necessary for these effects. The p190A-RasGAP interaction is mediated via FAK/Src phosphorylation of Tyr1087 and Tyr1105 in p190A, which creates docking sites for two SH2 domains in RasGAP that are separated by an SH3 domain (Figure S1C).[29–31] This interaction is abrogated by mutation of Tyr1087 and Tyr1105 in p190A to phenylalanines. Here, we abbreviate this double-mutant p190A(Y2F). In contrast to wild-type (WT) p190A, expression of p190A(Y2F) in H661 cells failed to activate LATS kinases or induce CIP, as determined by western blotting of total cell lysates to detect pLATS1/2(S909/S872) and cyclin A, respectively (Figures 1C and 1D). The requirement for p190A-RasGAP complex formation to induce CIP was further evidenced by quantification of cell number after seeding cells at sparse density. H661 cells expressing p190A(WT) reached a saturation density of ~3 million cells in a 35-mm dish or ~3×10^5 cells/cm^2. In contrast, control cells or cells expressing p190A(Y2F), as well H661-p190A cells with *RASA1*-KO, grew to significantly higher densities without the growth curve leveling out (Figure 1E). This difference in growth characteristics was also evidenced by confocal and phase microscopy. Only cells reconstituted with p190A(WT) grew in cobblestone-like monolayers, while control cells or cells with perturbed p190A-RasGAP complex formation exhibited cell multilayering (Figure 1F).

We furthermore tested the requirement for the p190A-RasGAP interaction to elicit MET. Unlike p190A(WT), expression of p190A(Y2F) did not promote an N- to E-cadherin switch (Figures 1G–1I). Moreover, p190A(Y2F) failed to downmodulate expression of the *TWIST1*, *ZEB1*, and *SNAIL2* genes that we previously have shown are suppressed by expression of p190A(WT) (Figure 1J).[20] Thus, formation of a p190A-RasGAP complex is required for LATS activation to elicit MET and promote CIP in H661 cells. Of note, we obtained very similar results with NSCLC NCI-H226 cells, thereby suggesting the general relevance of our findings (Figures S1E–S1I).

Interaction with RasGAP is necessary for the tumor-suppressor function of p190A

Next, we tested a role for the p190A-RasGAP interaction in tumor-suppressor function using a xenograft model that we previously established for p190A.[20] We injected 5×10^6 control H661 cells or cells expressing either p190A(WT) or p190A(Y2F) subcutaneously into the flank of nude mice. As previously reported,[20] mice injected with H661-p190A(WT) cells exhibited small tumors that rapidly regressed (Figure 2A). In contrast, mice injected with control cells or p190A(Y2F) cells showed aggressive tumor growth, which necessitated euthanasia after 4–10 weeks for all control mice and two-thirds of p190A(Y2F) mice (Figures 2A and 2B). The p190A(Y2F) tumors were slightly smaller than the control tumors, but the difference was statistically significant (Figure 2A). There were no obvious histological features to distinguish tumors formed by control and p190A(Y2F) cells (Figure S2A), with the exception that we detected staining for p190A in p190A(Y2F) but not control tumor cells (Figure S2B). Likewise, we did not observe overt differences in Ki-67 staining between control and p190A(Y2F) tumors (Figure S2C), which was verified by quantification (Figure S2D).

To compare tumors formed from cells expressing p190A(Y2F) to p190A(WT), we initiated a second cohort in which all mice were euthanized 3 weeks after injection of control, p190A(WT), or p190A(Y2F) cells. This analysis revealed that the central areas of p190A(WT) tumors were mostly composed of cellular debris and strands of eosinophilic material with the tumor cells lining the periphery (Figures 2C, S2E, and S2F). In contrast, control and p190A(Y2F) tumors were typically populated by cells both peripherally and internally (Figure 2C). Moreover, p190A protein was readily detected by immunohistochemistry (IHC) in both p190A(WT) and p190A(Y2F) tumors but was absent from controls (Figure 2D). Finally, staining for Ki-67 revealed that while p190A(WT) cells were quiescent, p190A(Y2F) cells were actively proliferating to an equal extent as control cells (Figures 2E and 2F). Taken together, these results demonstrate that direct interaction with RasGAP is necessary for the tumor-suppressor function of p190A.

ZO-1 and ZO-2 bind p190A in a RasGAP-dependent manner and dictate p190A localization

We then turned our attention to the interaction between p190A and ZO-1/2 identified by mass spectrometry. First, we validated the interaction. Using anti-Myc 9E10 antibody coupled to agarose beads, we performed immunoprecipitation from control and H661-p190A cells. Following SDS-PAGE of precipitated proteins and western blotting, we readily detected ZO-1 and ZO-2 in immunoprecipitates from H661-p190A cells but not control cells (Figure 3A). Second, we were able to immunoprecipitate endogenous p190A with transiently expressed FLAG-tagged ZO-2 from 293T cells (Figure S3A). Third, we verified that the interaction occurs between endogenously expressed p190A and ZO-1/2 proteins in mouse mammary epithelial EPH4 cells and Madin-Darby canine kidney MDCKII cells, as well as human mammary carcinoma MDA-MB-231 cells (Figures 3B and S3B). Fourth, we tested whether binding of p190A to RasGAP was necessary for the interaction with ZO-1/2 in H661 cells. Indeed, perturbation of the interaction between p190A and RasGAP, either by KO of *RASA1* or by expression of p190A(Y2F), obliterated the interaction between p190A and ZO-1/2 (Figure 3C). In contrast, KO of *TJP2* from H661-p190A cells did not impact the binding of RasGAP to p190A (Figure 3D).

Next, we probed the requirement for defined motifs in zonula occludens proteins for the interaction with p190A (Figure 3E). MDCKII cells with constitutive knockdown of ZO-1 and conditional expression of knockdown-resistant EGFP-tagged full-length ZO-1 or deletion mutants have been engineered and described by others.[32] From these cell lines, we performed immunoprecipitation with anti-p190A antibody followed by SDS-PAGE to detect relevant proteins by western blotting. The results shown in Figure 3F demonstrate that the carboxy-terminal GuK and ABR regions of ZO-1 are necessary for the interaction with p190A, while the N-terminal PDZ1 domain is dispensable. We moreover used this approach to determine that p190A binds to EGFP-tagged ZO-2 (Figure 3G), thus further supporting the data reported above. We were unable to immunoprecipitate ZO-3 with p190A, possibly because ZO-3 lacks an ABR (Figure 3E).

We have previously demonstrated that a fraction of p190A in MDCKII cells is associated with lateral membranes engaged in cell-cell contact.[19] Therefore, we examined whether ZO-1/2 mediates recruitment of p190A to these sites by confocal microscopy. Strikingly,

in cells depleted of ZO-2, p190A was localized in puncta scattered diffusely throughout the cytoplasm. Upon rescue with EGFP-tagged ZO-2, p190A showed intense staining of membranes engaged in cell-cell contact (Figures 3H and 3I). In contrast, cells depleted of ZO-1 did not exhibit substantially different localization of p190A relative to cells expressing knockdown-resistant EGFP-tagged ZO-1 (Figures 3H and 3I). Thus, ZO-2, but not ZO-1, promotes efficient targeting of p190A to lateral membranes. Attempts to determine whether ZO-1/2 control the subcellular localization of p190A in H226 and H661 cell lines have thus far been unsuccessful due to low-intensity staining. However, the data obtained with MDCKII cells establish that ZO-1 and ZO-2 not only bind to p190A but also that ZO-2 can dictate the subcellular localization of p190A.

Interaction with ZO-2 is necessary for p190A to activate LATS kinases, elicit MET, induce CIP, and suppress tumorigenesis

To test whether ZO-1/2 are required for tumor-suppressor functions of p190A, we generated control and H661-p190A(WT) cells with KO of *TJP1* or *TJP2*, encoding ZO-1 and ZO-2, respectively (Figures 4A, 4B, S3C–S3F, and S4A). To this end, we used a total of two single-guide RNAs (sgRNAs) targeting *TJP1* and *TJP2* each. Of note, KO of *TJP1* did not affect ZO-2 expression (Figure 4A). In contrast, KO of *TJP2* reduced ZO-1 levels (Figure 4B). The results of functional analyses revealed remarkable differences between *TJP1* and *TJP2* KOs. While *TJP1* KO was largely innocuous (Figure 4A), KO of *TJP2* abolished the capacity of p190A to activate LATS1/2, induce E-cadherin expression, and suppress cyclin A levels (Figures 4B, 4C, and S4A). Quantification of *CDH1* and *CDH2* transcripts further established that ZO-2 is essential for the N- to E-cadherin switch elicited by expression of p190A (Figure 4D). Accordingly, KO of *TJP2* to a greater extent than KO of *TJP1* abrogated the suppression of *TWIST1* and *ZEB1* transcripts observed upon restoring p190A expression in H661 cells (Figure S4B). Furthermore, in agreement with the effects on cyclin A levels, cell-proliferation assays demonstrated that *TJP2*, but not *TJP1*, is obligatory for p190A to induce CIP in H661 cells (Figure 4E). Moreover, KO of *TJP2*, but not *TJP1*, elicited multilayering of H661-p190A cells indistinguishable from control cells (Figure 4F). Collectively, these results demonstrate that ZO-2 is required for p190A to activate LATS kinases, promote MET, and induce CIP. However, we cannot formally exclude the possibility that partial depletion of ZO-1 contributes to the phenotype of *TJP2* KO cells.

E-cadherin is an established constituent of the Hippo pathway, which was originally demonstrated using mammary carcinoma MDA-MB-231 cells.[33] We subsequently determined that p190A induces expression of E-cadherin, which in turn is necessary for p190A to activate LATS kinases.[20] Vice versa, in MDA-MB-231 cells, p190A is obligatory for E-cadherin to promote LATS activation.[20] Here, we further queried whether ZO-2 is required for E-cadherin to activate LATS kinases. Indeed, KO of *TJP2* reduced LATS activation in MDA-MB-231 cells expressing E-cadherin (Figures S4C and S4D). Thus, both p190A and ZO-2 are essential for E-cadherin induction as well as activating the Hippo pathway. Moreover, ZO-2 is required for LATS1/2 activation upon forced expression of E-cadherin.

Next, we tested a role for ZO-2 in p190A-mediated tumor suppression in a xenograft assay. We injected nude mice with control or H661-p190A cells, as well as two clones of H661-p190A cells with CRISPR-Cas9-mediated KO of *TJP2*. As demonstrated repeatedly, expression of p190A in H661 cells attenuated tumorigenesis followed by complete shrinkage of tumors (Figure 4G). In contrast, H661-p190A cells with KO of *TJP2* formed tumors that were only slightly and insignificantly smaller than tumors from control cells (Figure 4G). The differences in survival between tumors resulting from inoculation of control and H661-p190A cells with *TJP2* KO were also marginal and not statistically significant (Figure 4H).

We performed a histological examination of tumors from a separate cohort in which all mice were euthanized 3 weeks after injection, again prior to the disappearance of tumors from mice injected with H661-p190A cells (Figure S4E). By IHC, we verified that p190A and ZO-2 were expressed as expected, i.e., that staining for p190A was absent from control cell tumors but present in H661-p190A cells with or without *TJP2*-KO (Figures S4E and S4F). Moreover, staining for ZO-2 was absent from tumors formed by H661-p190A cells with *TJP2*-KO but present in tumors from the two other groups (Figure S4G). Finally, we determined that while H661-p190A cells were quiescent, cells expressing p190A with *TJP2*-KO exhibited similar intensity and frequency of Ki-67 staining as control cells (Figures 4I and S4H). Thus, ZO-2 is obligatory for p190A-mediated tumor suppression.

Role of RasGAP interaction and ZO-2 in p190A-mediated effects on YAP activity and the cell cycle

We have previously established that p190A downmodulates the activity of the proto-oncogenic transcriptional co-activator to promote CIP.[19] Moreover, expression of p190A augments phosphorylation of YAP on Ser127, which inhibits translocation of YAP to the nucleus and transcriptional activity.[19] Here, we tested a requirement for RasGAP interaction and ZO-2 expression in these responses. We determined that pYAP(S127) levels were reduced by expression of p190A(Y2F) relative to p190A(WT) in H661 cells as well as by KO of *TJP2* in H661-p190A cells (Figures S5A and S5B). Accordingly, perturbation of RasGAP interaction or depletion of ZO-2 in p190A expressing H661 cells promoted translocation of YAP into the nucleus (Figures 5A and 5B). A similar effect was observed in H661-p190A cells depleted of LATS1 and LATS2 (Figures 5A and 5B). Intriguingly, the YAP staining showed a “honeycomb” pattern in H661-p190A cells suggestive of a localization to membranes engaged in cell-cell contact. In contrast to other perturbations, this pattern was not completely abolished by KO of *TJP2*. The latter may reflect the more complex role of ZO-2 on the Hippo pathway, as it extends to chaperoning YAP/TAZ in and out of the nucleus (Figures 5A and 5B).

Next, we tested the role of RasGAP interaction and ZO-2 expression in the capacity of p190A to repress cell proliferation at confluent cell density.[19] To this end, we performed 5-bromo-2′-deoxyuridine (BrdU) and 5-ethynyl-2′-deoxyuridine (EdU) incorporation assays analyzed by immunofluorescence and fluorescence-activated cell sorting (FACS), respectively. Perturbation of RasGAP binding significantly attenuated while depletion of ZO-2 or LATS1/2 completely abrogated the impact of p190A on BrdU/EdU incorporation,

while depletion of ZO-1 from H661-p190A cells showed an intermediate effect (Figures 5C, 5D, S5C, and S5D). These results correlated with elevated levels of CDK6 transcript and protein, as well as enhanced retinoblastoma (RB) phosphorylation in cells with perturbation of RasGAP interaction or KO of *TJP2* relative to H661-p190A cells (Figures 5E–5G and S5E). Furthermore, to formally test whether RasGAP binding and ZO-2 expression are necessary for p190A to promote CIP, we depleted YAP from p190A(Y2F) cells as well H661-p190A cells with *TJP2* KO. In both conditions, cyclin A levels were majorly reduced and cell proliferation significantly diminished (Figures 5H and 5I). These results were validated with verteporfin, an inhibitor of YAP-TEAD association (Figures 5J and 5K).[34] Taken together, these results establish that RasGAP interaction and ZO-2 expression are pivotal for p190A to promote CIP via enhanced phosphorylation and reduced nuclear translocation of YAP.

Finally, to test whether effects of p190A on the Hippo pathway extend to NSCLC cells without *ARHGAP35* alteration, we tested NCI-H2087 cells, which rank on top with respect to transcript levels of *ARHGAP35* (depmap.org). We depleted p190A from these cells, which virtually abolished and greatly attenuated phosphorylation of LATS1/2 and YAP, respectively (Figure S5F). In addition, p190A-mediated repression of YAP target gene expression was strikingly diminished (Figure S5G).

RasGAP and ZO-2 play essential roles in transcriptomic alterations elicited by p190A

In published studies, we have established that p190A exerts tumor-suppressor capacities via modulation of gene transcription. We therefore queried whether RasGAP and ZO-2 might influence transcriptomic alterations elicited by expression of p190A in H661 cells. To this end, we analyzed transcriptomes from control cells, p190A(WT)-expressing, or p190(Y2F)-expressing cells, as well as H661-p190A(WT) cells with or without KO of *TJP1* or *TJP2*. Given the results of our functional studies above, we compared gene expression in H661-p190A(WT) cells to each of the other conditions. The analysis revealed that gene expression in p190A(Y2F) cells is highly similar to that of control cells in terms of both number of genes up- or downmodulated and the identity of differentially expressed genes (DEGs). In total, 557 out of 1,153 (~48%) DEGs from control versus p190A(WT) and 557 out of 787 (~70%) DEGs from p190A(Y2F) versus p190A(WT) were regulated in a coordinate manner (Figures 6A, 6B, S6A, and S6B; Table S1). Moreover, in H661-p190A(WT) cells, *TJP2* modulates the expression of significantly more genes (1,750 DEGs) than *TJP1* (249 DEGs). Furthermore, the analysis reveals that gene expression in *TJP2*-KO cells is more dissimilar relative to control cells than cells expressing p190A(Y2F) (Figure S6B).

The Venn diagram in Figure 6A and the profile of DEGs of the four comparisons p190A(WT) vs. control, p190A(Y2F), p190A + *TJP1*-KO, and p190A + *TJP2*-KO demonstrates that there are many genes commonly regulated by control, p190(Y2F), and p190A(WT) + *TJP2*-KO while not regulated by p190A(WT) + *TJP1*-KO (Figures 6A and 6B). We therefore performed gene set enrichment analysis (GSEA) to identify shared gene signatures. To this end, we included the 50 hallmark gene sets from MSigDB and two customized Hippo signaling gene sets specific to H661 cells, which were generated from the most significantly altered genes when LATS1/2 were knocked down in H661-p190A

cells (Table S2). Of the 12 top pathways in this analysis, six pathways were completely conserved: Interferon-α (IFN-α) and IFN-γ responses, MTORC1 signaling, epithelial-to-mesenchymal transition (EMT), and the two Hippo signaling gene sets, i.e., LATS1/2-knockdown (KD) UP and LATS1/2-KD DN (Figure 6C). Putative roles for IFN-α and IFN-γ responses, as well as MTORC1 signaling, will be addressed elsewhere. Based on our prior work,[20] the presence of LATS1/2-KD UP, LATS1/2-KD-DN, and EMT signatures are highly reassuring. Accordingly, waterfall plots for control, p190A(Y2F), and p190A(WT) + *TJP2-KO* cells relative to cells expressing WT p190A only showed highly similar profiles (Figure 6D). Moreover, leading-edge analysis revealed the identity of genes that contribute most to the enrichment of the EMT gene set. We found strong similarity/common subgroup among the leading-edge genes that are modulated in p190A(Y2F) and p190A(WT) + *TJP2-KO* cells relative to p190A(WT) cells. The shared leading-edge genes are CDH2, GAS1, IGFBP3, MYLK, SCG2, SGCG, TAGLN, TGFBR3, and WIPF1 (Figure 6E). The commonality further extended to key individual Hippo signal genes (BIRC5 and CYR61) and EMT genes (*TWIST1*, *ZEB1*, CDH1, and CDH2) (Figure 6F). Finally, we mapped gene expression of 12 of the most significantly regulated genes in the LATS1/2-KD gene sets in control, p190A(Y2F), p190A(WT) + *TJP1-KO*, and p190A(WT) + *TJP2-KO* cells relative to cells expressing WT p190A only. For each of these genes, we observed modulation of gene expression consistent with the phenotypic alterations reported above (Figure S6C). Taken together, the transcriptomic data are highly consistent with the functional studies in establishing essential roles for RasGAP and ZO-2 in promoting tumor-suppressor capacities of p190A.

Expression of TJP1/2 differentiates survival of patients with *ARHGAP35* alteration in LUAD

We mined The Cancer Genome Atlas (TCGA) data for putative links between expression of *ARHGAP35* and *RASA1* as well as *TJP1* and *TJP2*. Given that our functional studies are conducted with NSCLC cells, we focused on LUAD, where *ARHGAP35* is frequently altered.[33] We collected four Hippo signaling gene sets from MSigDB and one customized H661 LATS1/2-KD gene set and analyzed the activity of Hippo signaling for each patient by gene set variation analysis (GSVA). Among LUAD patients, patients with high p190A expression levels have significantly higher scores of Hippo signaling activity than those with low p190A expression levels (Figures 7A and 7B). Moreover, there is a highly significant correlation between *ARHGAP35* expression levels in LUAD samples and Hippo signaling activity scores (Figure 7C). This observation provides crucial validation in human tumor samples of links between *ARHGAP35* and the Hippo pathway that we previously have established using cultured cells.[19,20] We then examined expression of *ARHGAP35* and *RASA1* as well as *TJP1* and *TJP2* in the TCGA database. We observed significant downmodulation *ARHGAP35*, *TJP1*, and *TJP2* in 524 primary tumors relative to 59 adjacent normal solid samples (Figure S7A). Next, we compared expression of *ARHGAP35* and *RASA1*, as well as *TJP1* and *TJP2*, in 59 paired tumor samples and uninvolved tissue from the same patients. Expression of *ARHGAP35*, *TJP1*, and *TJP2* were all significantly lower in tumor samples relative to matched uninvolved tissue (Figure 7D). In contrast, *RASA1* expression was significantly increased in tumor tissue (Figure 7D). Reasons for the latter observation are not clear but could be linked to the established role for RasGAP in angiogenesis.[34] Next, we stratified patients based on *TJP1/2* transcript levels

in tumors and queried the impact of *ARHGAP35* expression on survival in the respective patient populations. Strikingly, low *ARHGAP35* expression correlates with shorter survival in patients with high, but not low, transcript levels of *TJP1/2* irrespective of whether *ARHGAP35* altered samples were included or excluded (Figures 7E and S7B). This discovery is consistent with the requirement for ZO-2 in tumor-suppressor signaling elicited by p190A. The apparent role for ZO-1 might be due to cell-type-dependent differences in the respective roles of ZO-1 and ZO-2 for p190A function. Alternatively, it could also be explained by the strong positive correlation between *TJP1* and *TJP2* expression in the TCGA LUAD dataset (Figure S7C).

DISCUSSION

ARHGAP35 encoding p190A remains very sparingly studied in the context of cancer despite being highly altered by both deletion and mutation.[1–3] The spectrum of alterations is suggestive of a tumor-suppressor function. Accordingly, our past studies have determined that p190A is indeed a tumor suppressor and, consistently with this role, an upstream activator of the Hippo pathway.[19,20] Here, we aimed to define a physical link between p190A and established constituents of the Hippo pathway. To this end, we performed a mass spectrometry analysis to identify p190A interacting proteins in H661 cells in which we have shown that p190A activates LATS kinases. This analysis revealed RasGAP and zonula occludens proteins ZO-1/2 to rank among the most frequently interacting proteins.

A cDNA encoding p190A was originally cloned via the interaction with RasGAP, hence validating the results of our mass spectrometry analysis.[24] In the present study, we demonstrate that RasGAP is necessary for p190A to activate LATS kinases, elicit MET, induce CIP, and suppress tumorigenesis. This discovery is important because it expands the role of RasGAP as tumor suppressor. This finding is, moreover, consistent with RasGAP augmenting the GAP activity of p190A,[35] which is required for tumor-suppressor function.[20] Thus, the p190A-RasGAP complex may serve as a node for coordinating Hippo and Ras signaling. To this end, Campbell et al. strikingly demonstrated that *ARHGAP35*, *RASA1*, and *LATS1* rank among the most frequently altered genes in oncogene-negative LUAD.[36] Our present study establishes that p190A, RasGAP, and LATS1 signal in the same pathway. By inference, loss-of-function alterations in this pathway may drive oncogene-negative LUAD by activating YAP/TAZ transcriptional co-activators, which also have been shown to confer oncogenic capacities in Ras-resistant cancer.[37,38]

Next, we demonstrate that RasGAP is necessary for the interaction of p190A with the zonula occludens proteins ZO-1 and ZO-2 that serve as transcriptional modulators of ZONAB and TEAD transcription factors.[39,40] ZO-2, moreover, represents an integral constituent of the Hippo pathway via its direct interaction with YAP/TAZ and, potentially, LATS kinases.[41–43] Using MDCK cells expressing GFP-tagged ZO-1 and derivatives thereof, we demonstrate that p190A interacts with the C-terminal region of ZO-1 harboring the GuK and ABR motifs, i.e., distant from the PDZ1 domain in the N terminus that binds YAP/TAZ.[41,42] It remains to be determined whether the association between the p190A-RasGAP complex and ZO-1/2 is direct or indirect, which is not a trivial task due to the sheer size of the proteins and the number of motifs they contain. Moreover, we have hitherto been unable to determine

the subcellular localization of these constituents in the cancer cell lines studied herein. However, the observations with MDCK cells establish that ZO-2 possesses the capacity to dictate the subcellular localization of p190A to a site relevant to CIP. Functionally, our data demonstrate that ZO-2 is essential for p190A to activate LATS kinases, suppress YAP activity, elicit MET, induce CIP, and suppress tumorigenesis. ZO-2 is also required for E-cadherin to promote LATS activation, which we previously have shown to require p190A.[20] Furthermore, ZO-2 is necessary for the transcriptional response associated with tumor suppression elicited by expression of p190A. Finally, we determine that in LUAD samples where *ARHGAP35* expression correlates positively with Hippo signaling, low expression of *ARHGAP35* is associated with worse prognosis but only in patients with high *TJP2* expression in tumor tissue, consistent with *ARHGAP35* acting as a *TJP2*-dependent tumor-suppressor gene.

Work from other laboratories have established that Rho-ROCK-mediated actomyosin contraction represses activation of LATS kinases,[44–46] a mechanism that directly contributes to driving human malignancies.[47] This pathway, also referred to as mechanotransduction, attenuates direct binding between Nf2/Merlin and LATS kinases to promote YAP-mediated gene transcription.[48] Thus, inhibition of Rho signaling is essential to activate LATS kinases and promote growth control. Experimentally, this is typically achieved with global inhibitors of actin polymerization such as C3 toxin or latrunculin B. However, in physiological settings, Rho signaling must be fine-tuned to coordinate a vast array of processes, which requires simultaneous activation and inactivation of Rho activity at distinct subcellular sites.[49] Our past work has made p190A a strong candidate for a key enzyme to repress mechanotransduction in activation of LATS kinase.[19] Yet hitherto, we have been unable to identify a physical association between p190A and established constituents of the Hippo pathway. However, as summarized in the graphical abstract accompanying this article, our present demonstration of an interaction between the RasGAP-p190A complex and ZO-2 provides this missing link, such that the RasGAP-p190A complex can now be considered a bona fide constituent of the Hippo pathway. This is further supported by the demonstration by Cui et al. of a direct interaction between RasGAP and Nf2/Merlin,[50] although its significance to Hippo signaling remains to be determined.

In summary, this work elucidates a mechanism whereby the p190A-RasGAP complex via interaction with ZO-2 exerts tumor-suppressor capacities. From a rather obscure role in cancer, p190A is emerging as pivotal modulator of the Hippo pathway, with physical and functional links to established constituents of cell-cell junctions that are known to modulate the activities of LATS kinases and YAP/TAZ transcriptional co-activators.[51]

Limitations of the study

Work on the role of *ARHGAP35*/p190A in cancer is inherently limited by the relatively low number of publicly available tumor genome sequences, which precludes determination of significant co-occurring alterations and thus reverse engineering of genetically well-defined cell and mouse models. However, this caveat extends to other tumor-suppressor genes that are altered with single-digit percentages in human cancer and will be ameliorated over time as more tumor genomes are defined.[52]

STAR★METHODS

RESOURCE AVAILABILITY

Lead contact—Further information and requests for resources and reagents should be directed to and will be fulfilled by the lead contact, Steen H. Hansen (steen.hansen@childrens.harvard.edu). Please note that requester must defray actual costs of shipping.

Materials availability—Plasmids generated in this study are available from the lead contact, Steen H. Hansen (steen.hansen@childrens.harvard.edu). Please note that requester must defray actual costs of shipping.

Data and code availability

- All RNA-seq data have been deposited in NCBI's Gene Expression Omnibus and can be accessed using GEO Series accession number GSE212619.
- This paper does not report original code.
- Any additional information required to reanalyze the data reported in this work paper is available from the lead contact upon request.

EXPERIMENTAL MODEL AND STUDY PARTICIPANT DETAILS

Cell culture, transfection, transduction, and selection—NCI-H661 and NCI-H226 cell lines were propagated in DMEM/F12 1:1 supplemented with 10% FBS. 293T, MDA-MB-231, H2087 and MDCK cells were cultured in DMEM with 10% FCS. Transfections were performed using Omnifect or Fugene6 according to the manufacturer's instructions. For lentiviral transduction, one 100-mm dish with 70% confluent 239T cells was transfected with 2 μg each of VSV-G and PAX2 encoding plasmids, as well as 2-μg transfer vector. The medium was replaced after 24 h, and medium containing lentiviral particles harvested after 48 h. Following filtration through a 0.45-μm filter, the medium was supplemented with 8 μg/mL polybrene and added to target cells. Transduced cells were enriched either by FACS sorting for EGFP or mCherry expression, or by drug selection with 10 μg/mL blasticidin or 2 μg/mL puromycin for 10 days. Selected cells were expanded to generate frozen stock and then used for experimentation. For transient transfection, 6 μg plasmid and 18 μL Fugene6 were mixed in 1-mL of Opti-MEM. After incubation at room temperature for 15–30 min, the mixture was added to 100-mm dishes containing 70% confluent 293T cells in a total volume of 5 mL. The medium was replaced after 24 h and the cells processed for experimentation the following day.

Mice—6–7 weeks old female outbred homozygous nude Foxn1^{nu}/Foxn1^{nu} were obtained from The Jackson Laboratory Cat. no. 007850) and acclimatized for 2–3 days. Mice were then ear-tagged and injected with 100μL Matrigel containing 5×10^6 control or H661-p190A cells in the right flank. Mice were followed for up to 25 weeks after injection, during which weight and period tumor size (length × width) were measured 1–2 times per week and the condition of mice inspected. When tumors reached a maximum length of ≥8-mm, mice were euthanized by CO_2 asphyxiation per institutional guidelines and

tumors were removed for histology. These procedures were conducted according to BCH IACUC-approved protocol #3319. In parallel, smaller cohorts were established in which all mice, irrespective of tumor size were euthanized three weeks after injection of tumor cells.

METHOD DETAILS

Reagents—The following reagents were used for this work: Blasticidin (EMD Millipore); Calyculin A (Cell Signaling Technologies); DMEM (Corning); DMEM/F12 1:1 (Gibco); DRAQ5 (Biostatus); fetal bovine serum (FBS; Atlanta Biologicals); Luna Universal qPCR Master Mix (New England Biolabs); fish skin gelatin (Sigma-Aldrich); FluorSave (EMD Millipore); Fugene6 (Promega); goat serum (Gibco); Omnifect (Transomic technologies); PageRuler prestained protein ladder 10–180 kD (Thermo Fisher); puromycin (Sigma-Aldrich); phalloidin/Alexa ^{488} and phalloidin/Alexa ^{594} (Invitrogen); Polybrene (Santa Cruz Biotechnology); Puromycin (Sigma Aldrich); SuperSignal West Dura chemiluminescence reagent. Verteporfin (Beijing Biosynthesis Biotechnology Co.); Trypsin-EDTA, 0.25% (Gibco).

Antibodies—Antibodies used for this study were as follows.

Antigen	Species	Company	Cat. no.
β-actin	mouse monoclonal	Invitrogen	MA5-15739
BrdU	mouse monoclonal	Millipore-Sigma	MAB3222
Cdk6	mouse monoclonal	Cell Signaling Technologies	3136T
Cyclin A	rabbit polyclonal	Santa Cruz Biotechnologies	sc-751
E-Cadherin	mouse monoclonal	BD Biosciences	610182
ERK1	mouse monoclonal	Santa Cruz Biotechnologies	sc-271269
ERK1/2	rabbit polyclonal	Millipore-Sigma	M5670
FLAG-M2	mouse monoclonal	Millipore-Sigma	F3165
GFP	mouse monoclonal	Santa Cruz Biotechnologies	sc-9996
Ki-67	rabbit polyclonal	Thermo Fisher Scientific	RM9106S
pLATS1(S909)	rabbit monoclonal	Cell Signaling Technologies	9157S
LATS1	rabbit monoclonal	Cell Signaling Technologies	9153S
N-cadherin	mouse monoclonal	Cell Signaling Technologies	14215S
p190A	mouse monoclonal	BD Biosciences	610150
p190B	mouse monoclonal	BD Biosciences	611613
Rb	mouse monoclonal	Cell Signaling Technologies	9309T
pRB(S780)	rabbit monoclonal	Cell Signaling Technologies	8180T
pRB(S807/S811)	rabbit monoclonal	Cell Signaling Technologies	8516T
YAP1	rabbit polyclonal	Cell Signaling Technologies	9412S
pYAP1(S127)	rabbit polyclonal	Cell Signaling Technologies	4911S
ZO-1	rabbit monoclonal	Cell Signaling Technologies	8193S
ZO-1	rabbit monoclonal	Cell Signaling Technologies	13663S
ZO-1	rabbit polyclonal	Proteintech	21773-1-AP
ZO-2	rabbit monoclonal	Cell Signaling Technologies	2847S

Antigen	Species	Company	Cat. no.
ZO-2	rabbit polyclonal	Proteintech	18900-1-AP
ZO-2	rabbit polyclonal	Boster	PA1957

Secondary antibodies were the following: goat anti-mouse/Alexa ^{555} and goat anti-rabbit/Alexa ^{488} obtained from Invitrogen, as well as goat anti-mouse/HRP and goat anti-rabbit/HRP purchased from Jackson ImmunoResearch.

Plasmid constructs

Wild type p190A and p190A(Y2F) expression constructs were synthesized with an N-terminal Myc-tag by Genewiz and cloned into the lentiviral vector pUltra-hot from Addgene, plasmid #24130. The entire cDNAs for wild-type or p190A(Y2F) forms were verified by Sanger sequencing. ZO-2-FLAG and GFP-FLAG were generated by PCR, cloned into pLVX-EF1a-IRES-Puro and verified by Sanger sequencing in full. Lentiviral pZIP vectors encoding shRNAs targeting human p190A were purchased from transOMIC technologies Inc; cat. no. TRHS1000–35 (*ARHGAP35*/p190A) and validated as previously described.[19] YAP knockdown was performed by transducing cells with VectorBuilder pLV[shRNA]-Puro-U6>{shYAP553} with the following target sequence: GGTCAGAGAT ACTTCTTAAAT.

For CRISPR/Cas9-mediated knockout of *RASA1*, *TJP1* and *TJP2*, we utilized the following guide sequences:

RASA1 encoding p120 RasGAP

sgRNA#1 TCC CGT GTC GGG TGA AGA TAC CCG

sgRNA #2 TCC CTC TGG ATG GAC CAG AAT ACG.

TJP1 encoding ZO-1

sgRNA #1 TCC CGG AAA ATG ACC GAG TTG CAA

sgRNA #2 TCC CTG ACC GCC TGT CTG ACC GCG.

TJP2 encoding ZO-2

sgRNA #1 TCC CAC GGG TCT GGC AAC TAA AGA

sgRNA #2 ACC GAA AGA TGG CAA CCT TCA CGA

sgRNA#2 for *TJP2* in pLentiGuide-Puro was purchased from Addgene (#77828). All other sgRNAs were cloned into FgH1tUTG (Addgene #70183), which expresses EGFP for selection by FACS. To knock out gene expression using CRISPR/Cas9 methodology, CAS9 was first stably expressed from pLv5-Cas9-Neo in H661-control and H661-p190A cells. Next, such cells were transduced FgH1tUTG expressing sgRNAs under control of TetR. Expression of sgRNAs was then induced by 2 μg/mL doxycycline and pooled population of cells EGFP positive cells selected by FACS. Finally, for cells expressing *TJP2* sgRNA#1, clones were isolated and two

clones with no detectable ZO-2 expression used for a subset of experiments. Cells transduced with pLv5-Cas9-Neo only were used as controls for these experiments.

Immunoprecipitation and western blotting

These procedures were performed as previously described.[53] In brief, cells were rinsed with PBS and lysed in Gold lysis buffer (GLB) containing 137 mM NaCl, 30 mM Tris buffer pH 8.0, 5 mM EDTA, 15% glycerol and 1% Triton X-100 with addition of protease and phosphatase inhibitors. After lysis, nuclei were pelleted and the supernatant pre-cleared. Incubation with antibody was performed overnight followed by precipitation of antibody-antigen complexes with protein A/G Sepharose beads. After rinsing, bound proteins were eluted in Laemmli buffer and boiled for 3–5 min. Finally, samples and corresponding total cell lysates were subjected to SDS-PAGE and transferred to immobilon. Next, membranes were blocked in 5% milk in TBS-T, incubated with primary and secondary HRP-antibody followed by SuperSignal West Dura chemiluminescence reagent. Finally, imaging was performed with a ChemiDoc system.

Confocal microscopy

Samples were washed once with PBS and fixed in 3.7% formalin containing 1% methanol for 10 min at room temperature. After washing three times with PBS, samples were incubated 30 min in PBS containing 10% normal goat serum, 0.2% fish skin gelatin and 0.1% Triton X-100 (PBS-NGS). Next, samples were incubated with primary antibodies diluted in PBS-NGS for 1h, rinsed extensively with PBS containing 0.1% Triton X-100 for 30 min, and then incubated with secondary antibodies diluted in PBS-NGS for 40 min. Following additional extensive rinsing for 30 min, samples were stained for 15 min with DRAQ5 diluted 1:300 in PBS to detect nuclei and labeled with phalloidin/Alexa ^{488} or phalloidin/Alexa ^{594} to visualize polymerized actin. After final rinsing in PBS, samples were mounted with coverslips using FluorSave.

BrdU incorporation assay

BrdU was added to medium 100% confluent H661 cells for a final concentration of 3 μg/ml and incubated for 3 h at 37°C. Next, cells were fixed with 4% formalin in 0.1M phosphate buffer pH7.2 for 30 min at room temperature. Cells were then rinsed 5x with PBS over the course of 20 min followed by incubation in 2N HCl. Finally, cells were rinsed extensively with PBS before processing for immunofluorescence with anti-BrdU antibody and secondary according to the protocol summarized above.

EdU incorporation assay

This assay was conducted using the Click-iT EdU Pacific Blue kit (cat#C10418, Invitrogen). Briefly, H661 cells were seeded at 1 million per well in a 6-well plate and the medium was changed 24 h after seeding. The cells were cultured for another 48 h before EdU was added to the culture medium at a final concentration of 10 μM for 2 h. After 2 h, the cells were harvested by trypsinization. Next, the cells were fixed, permeabilized, and processed for the Click-iT reaction according to the manufacturer protocol. Finally, DRAQ5 was added for DNA stain before analysis by flow cytometry.

Histology

Tumors were removed from euthanized mice and fixed in 10% formalin overnight, dehydrated and embedded in Tissue Prep 2 paraffin. Samples were sectioned on a rotary microtome, and H&E staining was performed in an Autostainer. Retrieval of antigens was performed by boiling slides for 10 min in 10mM Sodium Citrate buffer in a pressure cooker. Sections were blocked with 5% normal donkey serum (Jackson ImmunoResearch Lab Inc, West Grove PA) for 1 h at room temperature. To quantify Ki-67, sections were incubated with rabbit anti-Ki-67 antibody overnight at 4°C. Sections were then washed in TBS/TBST and incubated with Alexa ^{488}-conjugated donkey anti-rabbit secondary antibody diluted 1:300. Next, sections were counter-stained with Hoechst 33342, washed with TBS/ TBST and mounted in Prolong Gold anti-fade mounting media (Invitrogen). Finally, Cell Profiler (Broad Institute) was used to define and count Ki-67 and Hoechst 33342 positive nuclei, respectively. Immunohistochemistry to detect p190A, ZO-2 and Ki-67 was performed using similar methods, except that incubation with primary antibodies was followed by HRP-conjugated goat anti-rabbit/mouse secondary antibody followed by staining with hematoxylin. H&E staining was performed using standard methods.

Real-time qPCR

Total RNA was extracted from cell pellets using Qiagen RNeasy Mini and QIAshredder kits according to the manufacturer's instructions. Next, cDNA was synthetized using Bio-Rad iScript cDNA Synthesis Kit according to the manufacturer's instructions. qRT-PCR was then performed with the One Step plus Sequence Detection System using Fast SYBR green master mix reagent. Experiments were performed either in quadruplicate of sextuplicate with half of the samples normalized to *HPRT* and the other half to *RPS18*. ΔΔCT Method was used in qPCR analysis. The average of the Ct values was calculated for the housekeeping gene and the gene of interest for each sample. Then the double delta Ct value (ΔΔCt) was calculated for every sample. Finally, the value of expression fold change was calculated by the formula of $2^{-\Delta\Delta Ct}$.

Primer sequences were as follows:

Gene	Forward primer (5′–3′)	Reverse primer (5′–3′)
AMOTL2	AGCTTCAATGAGGGTCTGCTC	CTGCTGAAGGACCTTGATCACT
ANKRD1	TGATTATGTATGGCGCGGATCT	GCGAGAGGTCTTGTAGGAGTTC
BIRC5	CCACTGAGAACGAGCCAGACTT	GTATTACAGGCGTAAGCCACCG
CDH1	GTCACTGACACCAACGATAATCCT	TTTCAGTGTGGTGATTACGACGTTA
CDH2	CCTCCAGAGTTTACTGCCATGAC	GTAGGATCTCCGCCACTGATTC
CTGF	GAAGCTGACCTGGAAGAGAACA	CGTCGGTACATACTCCACAGAA
CYR61	CATTCCTCTGTGTCCCCAAGAA	TACTATCCTCGTCACAGACCCA
DOCK4	ATGAGACCATCTTCCAGGCAGA	AGCTTTTGATGTTGTCCGGAAC
HPRT1	TTGCTTTCCTTGGTCAGGCA	ATCCAACACTTCGTGGGGTC
RND3	GGCCAGTTTTGAAATCGACACA	CAAATCAGCACAGCATCCGAAT
RPS18	CTTTGCCATCACTGCCATTAAG	TCCATCCTTTACATCCTTCTGTC

Gene	Forward primer (5′–3′)	Reverse primer (5′–3′)
SNAI2	ATCTGCGGCAAGGCGTTTTCCA	ATCTGCGGCAAGGCGTTTTCCA
TWIST1	GCCAGGTACATCGACTTCCTCT	TCCATCCTCCAGACCGAGAAGG
ZEB1	GGCATACACCTACTCAACTACGG	TGGGCGGTGTAGAATCAGAGTC

Genome-wide mRNA expression profiling

Transcriptome analysis was performed on the following H661 cell lines: H661 control, H661-p190A(WT), H661-p190A(WT)+*TJP1*-KO#1 and H661-p190A(WT)+*TJP2*-KO#1. Total RNA was isolated from 1×10^6 cells per sample using the RNeasy kit (Qiagen). Sample integrity was verified on an Agilent Technologies 2100 Bioanalyzer using the Agilent RNA 6000 Nano kit with an RNA integrity number (RIN) above 9.5 as threshold for acceptance. Next, samples were shipped to BGI Genomics Co. Ltd for further processing. In brief, total RNA was subjected to Oligo dT selection for enrichment of mRNA followed by reverse transcription and second strand synthesis. Following cDNA synthesis and library preparation, 50 bp end sequencing was performed on the BGISEQ-500 platform with a minimum of 20M clean reads per sample. Sequence reads were then filtered with SOAPnuke software to remove reads containing adaptors or unknown bases, as well as low-quality reads. Next, genome mapping of filtered reads to reference genome GRCh38 was performed using HISAT2 and Bowtie2 software.[54,55] Gene expression levels were calculated with RSEM.[56] Finally, differential gene expression was detected with NOIseq.[57]

RNA-seq data analysis and TCGA data analysis

Analyses andfigure generation were conducted within the RStudio software package using R version 3.63. Raw count data of RNA-seq were normalized and processed using R package DEseq2. Principal Components Analysis (PCA) was plotted using plotPCA function. Differentially expressed genes (DEGs) were analyzed using DESeq2. Genes with baseman >20, false discovery rate (FDR) < 0.05 and log2 (fold change) value > = 1 were considered significantly regulated. Hallmark gene sets were downloaded from MSigDB. We defined the customized LATS1/2-KD UP/DOWN gene sets from DEGs of LATS1/2 knockdown in H661-p190A expression cells, with the threshold set at baseMean >100, log2FoldChange ≥ 1 or <=−1, and p.adjust value ≤ 0.001. The 343 most up regulated genes were defined as LATS-KD UP gene set and the 239 most down regulated genes as LATS1/2-KD DN gene set. Gene set enrichment analysis (GSEA) was performed with Clusterprofiler package in R to determine the enrichment of pathways. The leading-edge genes contributed the most to the enrichment of EMT were obtained after running the standard GSEA analysis. The RNA-seq data are deposited in GEO submission GSE212619.

For the GDC TCGA Lung Adenocarcinoma (LUAD) cohort, both raw counts and processed FPKM-UQ data were downloaded from UCSC Xena Browser Datasets. RNA-seq data and matched clinical data were available for 524 primary tumors and 59 adjacent normal solid samples. FPKM-UQ normalized data were used for comparing the gene expression levels between tumor and normal tissues. Raw counts data were used as input and processed using

the GSVA package for analyzing Hippo pathway activity. The following four Hippo pathway gene sets were downloaded from MSigDB.

1. GOBP_HIPPO_SIGNALING
2. REACTOME_SIGNALING_BY_HIPPO
3. WP_HIPPO_SIGNALING_REGULATION_PATHWAYS
4. MCF10A_YAP1_DOWN.

The customized H661_p190A_LATS1/2 kd_DOWN geneset was defined as described in the RNA-seq part. Survival data were available for 511 patients of this cohort and was used for further survival analysis. Within the 511 samples, there are 16 samples with known missense/frameshift/stop-gained mutations for *ARHGAP35*, and 11 patients with replicate samples.

QUANTIFICATION AND STATISTICAL ANALYSIS

Experiments were performed in biological triplicate or higher as indicated in Figure Legends. Student t tests (unpaired, two-tailed, unequal variance) and log rank tests were performed as described previously.[58] In all figures *, **, ***, and **** denote $p < 0.05$, 0.025, 0.01, and 0.001 respectively, while not significantly different is abbreviated “nsd”.

Supplementary Material

Refer to Web version on PubMed Central for supplementary material.

ACKNOWLEDGMENTS

We are grateful to Jerrold R. Turner for providing MDCK cell lines expressing GFP-tagged ZO proteins, Phi Luong for critical reading of the manuscript, and Suzanne L. White and Dr. Lay-Hong Ang, BIDMC confocal imaging and IHC core, for assistance with histology procedures. This work utilized Harvard Digestive Diseases Center core facilities (NIH P30DK034854) and was funded primarily by NIH R01 CA205158, as well as an endowed chair from the Roy and Lynne Frank Foundation (to S.H.H.). Additional funding was obtained from the National Natural Science Foundation of China 82101989 and Guangdong Basic and Applied Basic Research Foundation 2019A1515111170 (to S.W.).

REFERENCES

1. Lawrence MS, Stojanov P, Mermel CH, Robinson JT, Garraway LA, Golub TR, Meyerson M, Gabriel SB, Lander ES, and Getz G (2014). Discovery and saturation analysis of cancer genes across 21 tumour types. Nature 505, 495–501. [PubMed: 24390350]
2. Kandoth C, McLellan MD, Vandin F, Ye K, Niu B, Lu C, Xie M, Zhang Q, McMichael JF, Wyczalkowski MA, et al. (2013). Mutational landscape and significance across 12 major cancer types. Nature 502, 333–339. [PubMed: 24132290]
3. Zack TI, Schumacher SE, Carter SL, Cherniack AD, Saksena G, Tabak B, Lawrence MS, Zhsng C-Z, Wala J, Mermel CH, et al. (2013). Pan-cancer patterns of somatic copy number alteration. Nat. Genet 45, 1134–1140. [PubMed: 24071852]
4. Dou Y, Kawaler EA, Cui Zhou D, Gritsenko MA, Huang C, Blumen-berg L, Karpova A, Petyuk VA, Savage SR, Satpathy S, et al. (2020). Proteogenomic Characterization of Endometrial Carcinoma. Cell 180, 729–748.e26. [PubMed: 32059776]
5. Xie SN, Cai YJ, Ma B, Xu Y, Qian P, Zhou JD, Zhao FG, and Chen J (2019). The genomic mutation spectrums of breast fibroadenomas in Chinese population by whole exome sequencing analysis. Cancer Med. 8, 2372–2379. [PubMed: 30851086]

6. Reyna MA, Haan D, Paczkowska M, Verbeke LPC, Vazquez M, Kahraman A, Pulido-Tamayo S, Barenboim J, Wadi L, Dhingra P, et al. (2020). Pathway and network analysis of more than 2500 whole cancer genomes. Nat. Commun 11, 729. [PubMed: 32024854]
7. Rajendran BK, and Deng C-X (2017). Characterization of potential driver mutations involved in human breast cancer by computational approaches. Oncotarget 8, 50252–50272. [PubMed: 28477017]
8. Cherniack AD, Shen H, Walter V, Stewart C, Murray BA, Bowlby R, Hu X, Ling S, Soslow RA, Broaddus RR, et al. (2017). Integrated Molecular Characterization of Uterine Carcinosarcoma. Cancer Cell 31, 411–423. [PubMed: 28292439]
9. Benna C, Simioni A, Pasquali S, De Boni D, Rajendran S, Spiro G, Colombo C, Virgone C, DuBois SG, Gronchi A, et al. (2018). Genetic susceptibility to bone and soft tissue sarcomas: a field synopsis and meta-analysis. Oncotarget 9, 18607–18626. [PubMed: 29719630]
10. Zhang Y, Zhang L, Li R, Chang DW, Ye Y, Minna JD, Roth JA, Han B, and Wu X (2017). Genetic variations in cancer-related significantly mutated genes and lung cancer susceptibility. Ann. Oncol 28, 1625–1630. [PubMed: 28383694]
11. Knijnenburg TA, Bismeijer T, Wessels LFA, and Shmulevich I (2015). A multilevel pan-cancer map links gene mutations to cancer hall-marks. Chin. J. Cancer 34, 439–449. [PubMed: 26369414]
12. Sanchez-Vega F, Mina M, Armenia J, Chatila WK, Luna A, La KC, Dimitriadoy S, Liu DL, Kantheti HS, Saghafinia S, et al. (2018). Oncogenic Signaling Pathways in The Cancer Genome Atlas. Cell 173, 321–337.e10. [PubMed: 29625050]
13. Gopal RK, Kübler K, Calvo SE, Polak P, Livitz D, Rosebrock D, Sadow PM, Campbell B, Donovan SE, Amin S, et al. (2018). Wide-spread Chromosomal Losses and Mitochondrial DNA Alterations as Genetic Drivers in Hürthle Cell Carcinoma. Cancer Cell 34, 242–255.e5. [PubMed: 30107175]
14. Wang Y, Yu M, Yang J-X, Cao D-Y, Zhang Y, Zhou H-M, Yuan Z, and Shen K (2019). Genomic Comparison of Endometrioid Endometrial Carcinoma and Its Precancerous Lesions in Chinese Patients by High-Depth Next Generation Sequencing. Front. Oncol 9, 123. [PubMed: 30886832]
15. Settleman J, Albright CF, Foster LC, and Weinberg RA (1992). Association between GTPase activators for Rho and Ras families. Nature 359, 153–154. [PubMed: 1522900]
16. Ligeti E, Dagher M-C, Hernandez SE, Koleske AJ, and Settleman J (2004). Phospholipids can switch the GTPase substrate preference of a GTPase-activating protein. J. Biol. Chem 279, 5055–5058. [PubMed: 14699145]
17. Wennerberg K, Forget M-A, Ellerbroek SM, Arthur WT, Burridge K, Settleman J, Der CJ, and Hansen SH (2003). Rnd proteins function as RhoA antagonists by activating p190 RhoGAP. Curr. Biol 13, 1106–1115. [PubMed: 12842009]
18. Jiang W, Sordella R, Chen G-C, Hakre S, Roy AL, and Settleman J (2005). An FF domain-dependent protein interaction mediates a signaling pathway for growth factor-induced gene expression. Mol. Cell 17, 23–35. [PubMed: 15629714]
19. Frank SR, Köllmann CP, Luong P, Galli GG, Zou L, Bernards A, Getz G, Calogero RA, Frödin M, and Hansen SH (2018). p190 RhoGAP promotes contact inhibition in epithelial cells by repressing YAP activity. J. Cell Biol 217, 3183–3201. [PubMed: 29934311]
20. Ouyang H, Luong P, Frödin M, and Hansen SH (2020). p190A RhoGAP induces CDH1 expression and cooperates with E-cadherin to activate LATS kinases and suppress tumor cell growth. Oncogene 39, 5570–5587. [PubMed: 32641858]
21. Héraud C, Pinault M, Lagrée V, and Moreau V (2019). p190RhoGAPs, the ARHGAP35- and ARHGAP5-Encoded Proteins, in Health and Disease. Cells 8, E351.
22. Zhang Y, Li Y, Wang Q, Su B, Xu H, Sun Y, Sun P, Li R, Peng X, and Cai J (2020). Role of RASA1 in cancer: A review and update (Review). Oncol. Rep 44, 2386–2396. [PubMed: 33125148]
23. González-Mariscal L, Gallego-Gutiérrez H, González-González L, and Hernández-Guzmán C (2019). ZO-2 Is a Master Regulator of Gene Expression, Cell Proliferation, Cytoarchitecture, and Cell Size. Indian J. Manag. Sci 20, 4128.

24. Settleman J, Narasimhan V, Foster LC, and Weinberg RA (1992). Molecular cloning of cDNAs encoding the GAP-associated protein p190: implications for a signaling pathway from ras to the nucleus. Cell 69, 539–549. [PubMed: 1581965]
25. Willott E, Balda MS, Fanning AS, Jameson B, Van Itallie C, and Anderson JM (1993). The tight junction protein ZO-1 is homologous to the Drosophila discs-large tumor suppressor protein of septate junctions. Proc. Natl. Acad. Sci. USA 90, 7834–7838. [PubMed: 8395056]
26. Jesaitis LA, and Goodenough DA (1994). Molecular characterization and tissue distribution of ZO-2, a tight junction protein homologous to ZO-1 and the Drosophila discs-large tumor suppressor protein. J. Cell Biol 124, 949–961. [PubMed: 8132716]
27. Kulkarni SV, Gish G, van der Geer P, Henkemeyer M, and Pawson T (2000). Role of p120 Ras-GAP in directed cell movement. J. Cell Biol 149, 457–470. [PubMed: 10769036]
28. Tomar A, Lim S-T, Lim Y, and Schlaepfer DD (2009). A FAK-p120RasGAP-p190RhoGAP complex regulates polarity in migrating cells. J. Cell Sci 122, 1852–1862. [PubMed: 19435801]
29. Bryant SS, Briggs S, Smithgall TE, Martin GA, McCormick F, Chang JH, Parsons SJ, and Jove R (1995). Two SH2 domains of p120 Ras GTPase-activating protein bind synergistically to tyrosine phosphorylated p190 Rho GTPase-activating protein. J. Biol. Chem 270, 17947–17952. [PubMed: 7629101]
30. Hu KQ, and Settleman J (1997). Tandem SH2 binding sites mediate the RasGAP-RhoGAP interaction: a conformational mechanism for SH3 domain regulation. EMBO J. 16, 473–483. [PubMed: 9034330]
31. van der Geer P, Henkemeyer M, Jacks T, and Pawson T (1997). Aberrant Ras regulation and reduced p190 tyrosine phosphorylation in cells lacking p120-Gap. Mol. Cell Biol 17, 1840–1847. [PubMed: 9121432]
32. Odenwald MA, Choi W, Buckley A, Shashikanth N, Joseph NE, Wang Y, Warren MH, Buschmann MM, Pavlyuk R, Hildebrand J, et al. (2017). ZO-1 interactions with F-actin and occludin direct epithelial polarization and single lumen specification in 3D culture. J. Cell Sci 130, 243–259. [PubMed: 27802160]
33. Kim N-G, Koh E, Chen X, and Gumbiner BM (2011). E-cadherin mediates contact inhibition of proliferation through Hippo signaling-pathway components. Proc. Natl. Acad. Sci. USA 108, 11930–11935. [PubMed: 21730131]
34. Liu-Chittenden Y, Huang B, Shim JS, Chen Q, Lee S-J, Anders RA, Liu JO, and Pan D (2012). Genetic and pharmacological disruption of the TEAD-YAP complex suppresses the oncogenic activity of YAP. Genes Dev. 26, 1300–1305. [PubMed: 22677547]
35. Haskell MD, Nickles AL, Agati JM, Su L, Dukes BD, and Parsons SJ (2001). Phosphorylation of p190 on Tyr1105 by c-Src is necessary but not sufficient for EGF-induced actin disassembly in C3H10T1/2 fibro-blasts. J. Cell Sci 114, 1699–1708. [PubMed: 11309200]
36. Campbell JD, Alexandrov A, Kim J, Wala J, Berger AH, Pedamallu CS, Shukla SA, Guo G, Brooks AN, Murray BA, et al. (2016). Distinct patterns of somatic genome alterations in lung adenocarcinomas and squamous cell carcinomas. Nat. Genet 48, 607–616. [PubMed: 27158780]
37. Shao DD, Xue W, Krall EB, Bhutkar A, Piccioni F, Wang X, Schinzel AC, Sood S, Rosenbluh J, Kim JW, et al. (2014). KRAS and YAP1 converge to regulate EMT and tumor survival. Cell 158, 171–184. [PubMed: 24954536]
38. Kapoor A, Yao W, Ying H, Hua S, Liewen A, Wang Q, Zhong Y, Wu C-J, Sadanandam A, Hu B, et al. (2014). Yap1 activation enables bypass of oncogenic Kras addiction in pancreatic cancer. Cell 158, 185–197. [PubMed: 24954535]
39. Balda MS, and Matter K (2000). The tight junction protein ZO-1 and an interacting transcription factor regulate ErbB-2 expression. EMBO J. 19, 2024–2033. [PubMed: 10790369]
40. Gallego-Gutiérrez H, González-González L, Ramírez-Martínez L, López-Bayghen E, and González-Mariscal L (2021). Tight junction protein ZO-2 modulates the nuclear accumulation of transcription factor TEAD. Mol. Biol. Cell 32, 1347–1358. [PubMed: 34010016]
41. Oka T, Remue E, Meerschaert K, Vanloo B, Boucherie C, Gfeller D, Bader GD, Sidhu SS, Vandekerckhove J, Gettemans J, and Sudol M (2010). Functional complexes between YAP2 and ZO-2 are PDZ domain-dependent, and regulate YAP2 nuclear localization and signalling. Biochem. J 432, 461–472. [PubMed: 20868367]

42. Remue E, Meerschaert K, Oka T, Boucherie C, Vandekerckhove J, Sudol M, and Gettemans J (2010). TAZ interacts with zonula occludens-1 and −2 proteins in a PDZ-1 dependent manner. FEBS Lett. 584, 4175–4180. [PubMed: 20850437]
43. Xu J, Kausalya PJ, Ong AGM, Goh CMF, Mohamed Ali S, and Hunziker W (2022). ZO-2/*TJP2* suppresses Yap and Wwtr1/Taz-mediated hepatocyte to cholangiocyte transdifferentiation in the mouse liver. NPJ Regen. Med 7, 55. [PubMed: 36151109]
44. Dupont S, Morsut L, Aragona M, Enzo E, Giulitti S, Cordenonsi M, Zanconato F, Le Digabel J, Forcato M, Bicciato S, et al. (2011). Role of YAP/TAZ in mechanotransduction. Nature 474, 179–183. [PubMed: 21654799]
45. Aragona M, Panciera T, Manfrin A, Giulitti S, Michielin F, Elvassore N, Dupont S, and Piccolo S (2013). A Mechanical Checkpoint Controls Multicellular Growth through YAP/TAZ Regulation by Actin-Processing Factors. Cell 154, 1047–1059. [PubMed: 23954413]
46. Yu F-X, Zhang Y, Park HW, Jewell JL, Chen Q, Deng Y, Pan D, Taylor SS, Lai Z-C, and Guan K-L (2013). Protein kinase A activates the Hippo pathway to modulate cell proliferation and differentiation. Genes Dev. 27, 1223–1232. [PubMed: 23752589]
47. Esposito D, Pant I, Shen Y, Qiao RF, Yang X, Bai Y, Jin J, Poulikakos PI, and Aaronson SA (2022). ROCK1 mechano-signaling dependency of human malignancies driven by TEAD/YAP activation. Nat. Commun 13, 703. [PubMed: 35121738]
48. Yin F, Yu J, Zheng Y, Chen Q, Zhang N, and Pan D (2013). Spatial organization of Hippo signaling at the plasma membrane mediated by the tumor suppressor Merlin/NF2. Cell 154, 1342–1355. [PubMed: 24012335]
49. Fritz RD, and Pertz O (2016). The dynamics of spatio-temporal Rho GTPase signaling: formation of signaling patterns. F1000Res. 5. F1000 Faculty Rev-749.
50. Cui Y, Groth S, Troutman S, Carlstedt A, Sperka T, Riecken LB, Kissil JL, Jin H, and Morrison H (2019). The NF2 tumor suppressor merlin interacts with Ras and RasGAP, which may modulate Ras signaling. Oncogene 38, 6370–6381. [PubMed: 31312020]
51. Karaman R, and Halder G (2018). Cell Junctions in Hippo Signaling. Cold Spring Harbor Perspect. Biol 10, a028753.
52. Canisius S, Martens JWM, and Wessels LFA (2016). A novel independence test for somatic alterations in cancer shows that biology drives mutual exclusivity but chance explains most co-occurrence. Genome Biol. 17, 261. [PubMed: 27986087]
53. Hansen SH, Zegers MM, Woodrow M, Rodriguez-Viciana P, Chardin P, Mostov KE, and McMahon M (2000). Induced expression of Rnd3 is associated with transformation of polarized epithelial cells by the Raf-MEK-extracellular signal-regulated kinase pathway. Mol. Cell Biol 20, 9364–9375. [PubMed: 11094087]
54. Kim D, Langmead B, and Salzberg SL (2015). HISAT: a fast spliced aligner with low memory requirements. Nat. Methods 12, 357–360. [PubMed: 25751142]
55. Langmead B, and Salzberg SL (2012). Fast gapped-read alignment with Bowtie 2. Nat. Methods 9, 357–359. [PubMed: 22388286]
56. Li B, and Dewey CN (2011). RSEM: accurate transcript quantification from RNA-Seq data with or without a reference genome. BMC Bioinf. 12, 323.
57. Tarazona S, García-Alcalde F, Dopazo J, Ferrer A, and Conesa A (2011). Differential expression in RNA-seq: a matter of depth. Genome Res. 21, 2213–2223. [PubMed: 21903743]
58. Frank SR, Köllmann CP, van Lidth de Jeude JF, Thiagarajah JR, Engelholm LH, Frödin M, and Hansen SH (2017). The focal adhesion-associated proteins DOCK5 and GIT2 comprise a rheostat in control of epithelial invasion. Oncogene 36, 1816–1828. [PubMed: 27669437]

Highlights

- *ARHGAP35* is a human TSG encoding p190A RhoGAP, an activator of the Hippo pathway
- Interactions of p190A with RasGAP and ZO-2 are necessary to activate LATS kinases
- RasGAP/ZO-2 are required for effects of p190A on gene expression and tumorigenesis
- *ARHGAP35* expression in LUAD samples correlates strongly with Hippo signaling

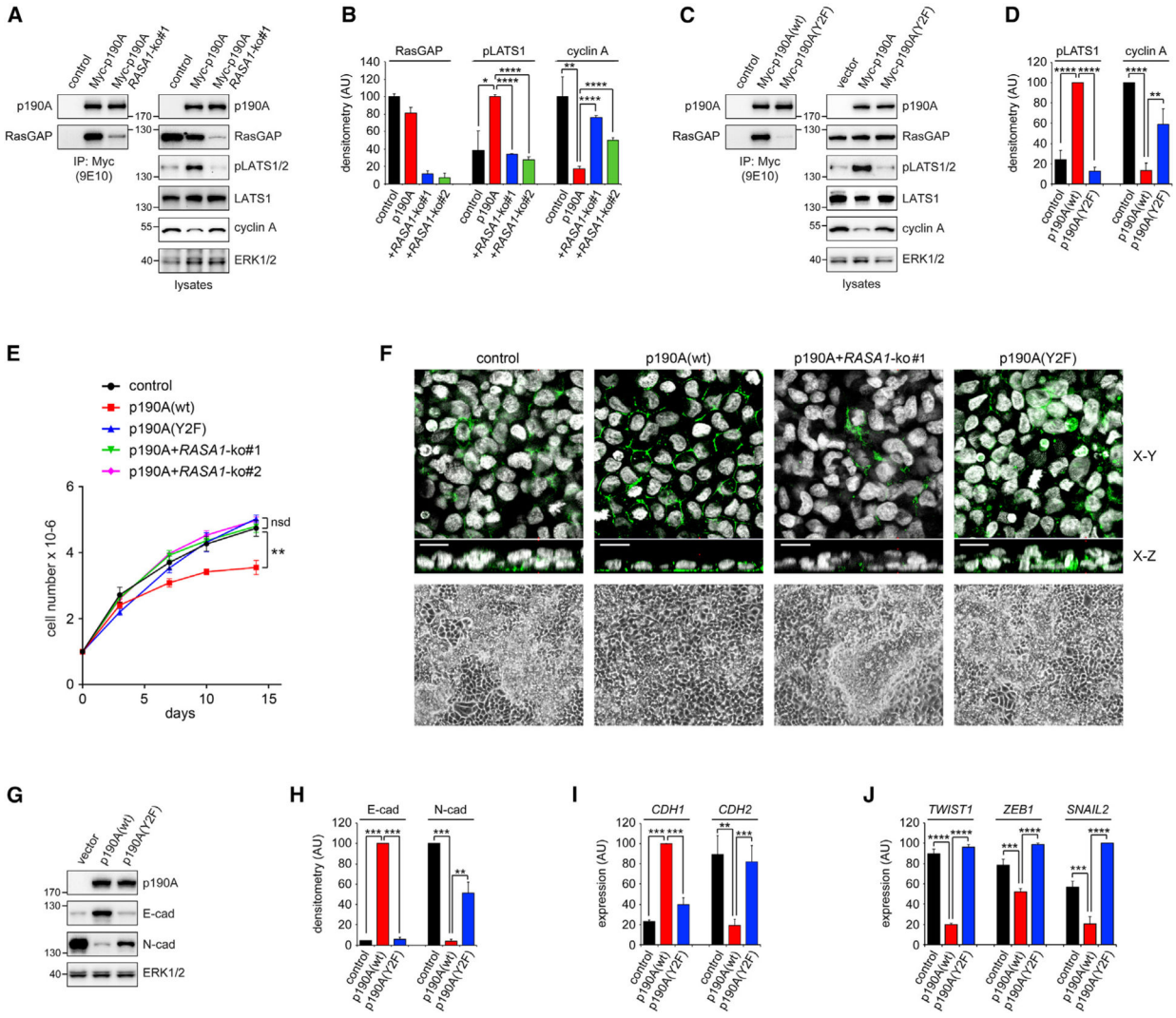

Figure 1. Interaction of p190A with RasGAP is necessary for p190A to activate of LATS1 kinase, promote CIP, and elicit MET

(A) Western blots of co-immunoprecipitations (coIPs) and corresponding whole-cell lysates to detect p190A, RasGAP, pLATS1/2, LATS1, cyclin A and ERK1/2 in control H661 cells, as well as H661-p190A cells expressing *RASA1* sgRNA#1.

(B) Quantification by densitometry of RasGAP, pLATS1/2, and cyclin A levels detected by western blotting as shown in (A). Data are presented as mean ± SD (n = 3).

(C) Western blots of coIPs and corresponding whole-cell lysates to detect p190A, RasGAP, pLATS1/2, LATS, cyclin A, and ERK1/2 in control cells, as well as H661 cells reconstituted with either p190A(WT) or p190A(Y2F) defective in RasGAP binding.

(D) Quantification by densitometry of RasGAP, pLATS1/2, and cyclin A levels detected by western blotting as shown in (C). Data are presented as mean ± SD (n = 3).

(E) Growth curves for control and H661 cells reconstituted with p190A(WT) or p190A(Y2F), ±*RASA1* KO. 1×10^6 cells were seeded per well of a 6-well plate in triplicate and propagated for the number of days indicated with a change of medium every 2 days. Cell number was quantified manually. Data are presented as mean ± SD.

(F) Interaction with RasGAP is necessary for p190A to restore monolayer architecture. Top panels show confocal microscopy of control cells, as well as H661 cells with expression of p190A(WT) ±*RASA1* KO or p190A(Y2F). Cells are labeled with fluorescent phalloidin (green) and the DNA-binding dye DRAQ5 (white). Scale bars represent 10 μm. The bottom panels show phase images for the same conditions.

(G) Western blots of whole-cell lysates to detect p190A, E-cadherin, N-cadherin, and ERK1/2 in control cells, as well as H661 reconstituted with either WT p190A or p190A(Y2F).

(H) Quantification by densitometry of E-cadherin, and N-cadherin levels detected by western blotting as shown in (G). Data are presented as mean ± SD (n = 3).

(I) Transcript levels for *CDH1* and *CDH2*, as determined by qPCR. Data are presented as mean ± SD (n = 4).

(J) Transcript levels for *TWIST1*, *ZEB1*, and *SNAIL2*, as determined by qPCR. Data are presented as mean ± SD (n = 4). All statistical testing for data presented was performed using pairwise Student's t test as indicated by brackets.

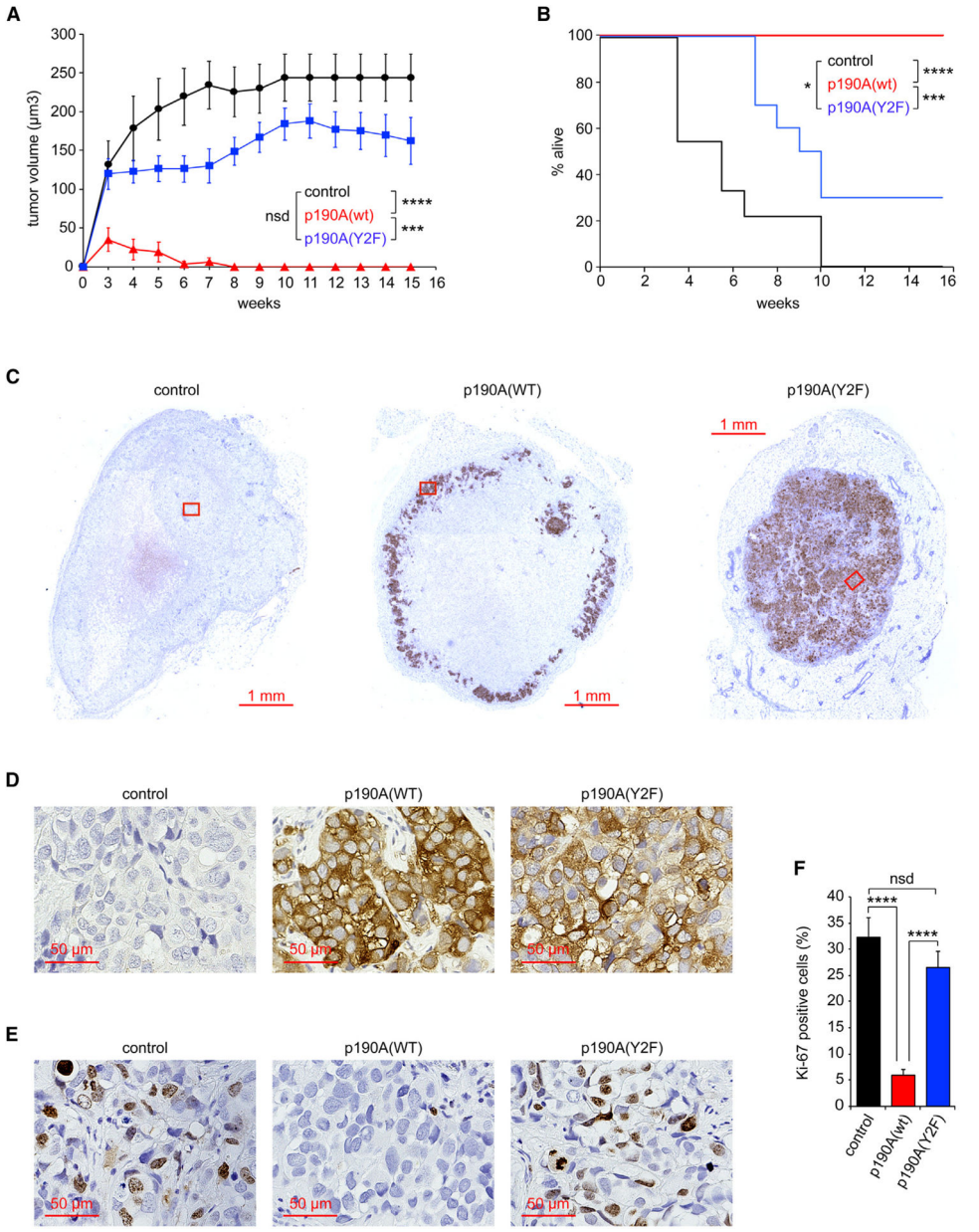

Figure 2. Interaction of p190A with RasGAP is required for the tumor-suppressor function of p190A

(A) Cumulative xenograft tumor volume in mice injected with control cells (n = 9) or H661 cells expressing p190A(WT) (n = 10) or p190A(Y2F) (n = 10). Data are presented as mean ± SEM. Statistical testing was performed using pairwise Student's t test as indicated by brackets.

(B) Kaplan-Meier survival plot for mice the cohort of mice described in (A). Statistical testing was performed using pairwise log-rank test as indicated by brackets.

(C) Immunohistochemistry to detect p190A in tumors 3 weeks after injection of control cells or H661 cells expressing p190A(WT) or p190A(Y2F).

(D) 20× magnifications of the areas contained within the red boxes in (C).

(E) Immunohistochemistry to detect Ki-67 positive cells in tumors 3 weeks after injection of control cells or H661 cells expressing p190A(WT) or p190A(Y2F).
(F) Quantification of Ki-67 positive cells from (E). Data are presented as mean ± SEM with n = 5 mice and >600 nuclei scored per condition. Statistical testing was performed using pairwise Student's t test as indicated by brackets.

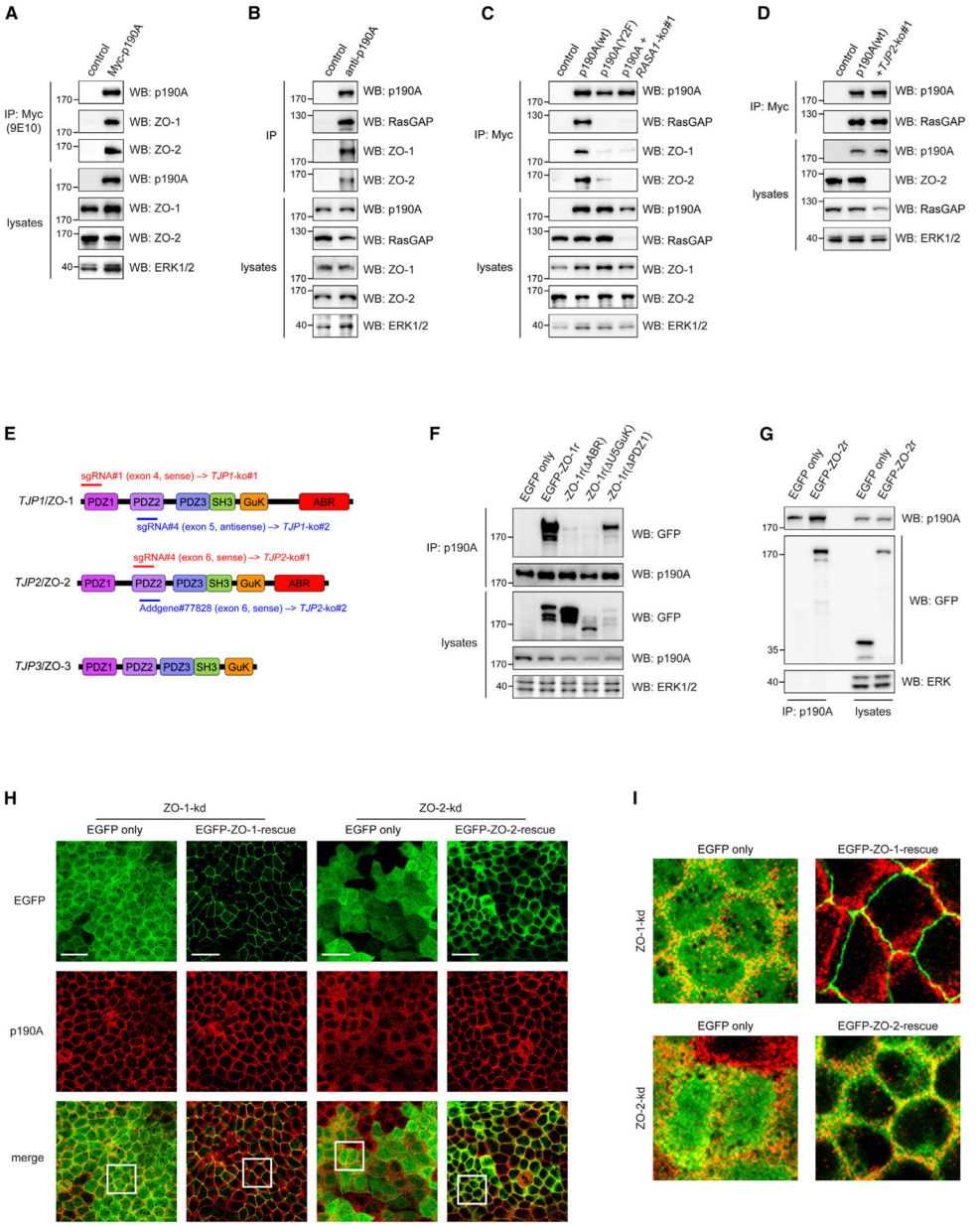

Figure 3. ZO-1/2 bind p190A in a RasGAP-dependent manner and recruit p190A to the plasma membrane

(A) Validation of the interaction between p190A and ZO-1/2 detected by mass spectrometry. Confluent cultures of control cells and H661 expressing Myc-tagged p190A cells were lysed in gold lysis buffer and processed for immunoprecipitation (IP) using mouse monoclonal 9E10 anti-Myc epitope antibody immobilized on agarose beads followed by western blotting (WB) to detect p190A, ZO-1, ZO-2, and ERK1/2.

(B) Confluent cultures of MDA-MB-231 cells were processed for immunoprecipitation with rabbit polyclonal anti-p190A antibody or without antibody followed by protein A/G Sepharose beads. Next, p190A, RasGAP, ZO-1, ZO-2, and ERK1/2 were detected in immunoprecipitates and lysates by western blotting.

(C) ZO-1 and ZO-2 bind p190A in a RasGAP-dependent manner. Confluent cultures of control cells or H661 cells expressing Myc-tagged p190A(WT) ± *RASA1*-KO or p190A(Y2F) were processed for immunoprecipitation with 9E10 antibody followed by western blotting to detect p190A, RasGAP, ZO-1, ZO-2, and ERK1/2.

(D) Binding of p190A to RasGAP is independent of ZO-2. Confluent cultures of control cells or H661 cells expressing Myc-tagged p190A ± *TJP2-KO* were processed for immunoprecipitation with 9E10 antibody followed by western blotting to detect p190A, RasGAP, ZO-2, and ERK1/2.

(E and F) The U5GuK and ABR domains of ZO-1 are necessary for the interaction with p190A. (E) Cartoon depicting domain structure of zonula occludens proteins ZO-1, ZO-2, and ZO-3. The regions encoded by ZO-1 and ZO-2 sequences targeted by sgRNAs are marked. (F) MDCK II cells depleted of endogenous ZO-1 and expressing exogenous EGFP only or knockdown-resistant EGFP-tagged full-length ZO-1 or ZO-1 deletion mutant missing the ABR, U5GuK, or PDZ1 domains were processed for immunoprecipitation with polyclonal rabbit anti-p190A antibody followed by western blotting to detect GFP, p190A, and ERK1/2.

(G) Interaction of ZO-2 with p190A in MDCK cells. MDCK II cells depleted of endogenous ZO-2 and expressing exogenous EGFP only or knockdown-resistant EGFP-tagged full-length ZO-2 were processed for immunoprecipitation with polyclonal p190A antibody followed by western blotting to detect GFP and p190A.

(H) Immunofluorescence to detect p190A (red) in MDCK II cell depleted of ZO-1 or ZO-2 expressing either EGFP alone or knockdown-resistant EGFP-tagged full-length ZO-1 or ZO-2 as indicated. Scale bars represent 10 μm.

(I) 5× magnification of the boxed areas in (H).

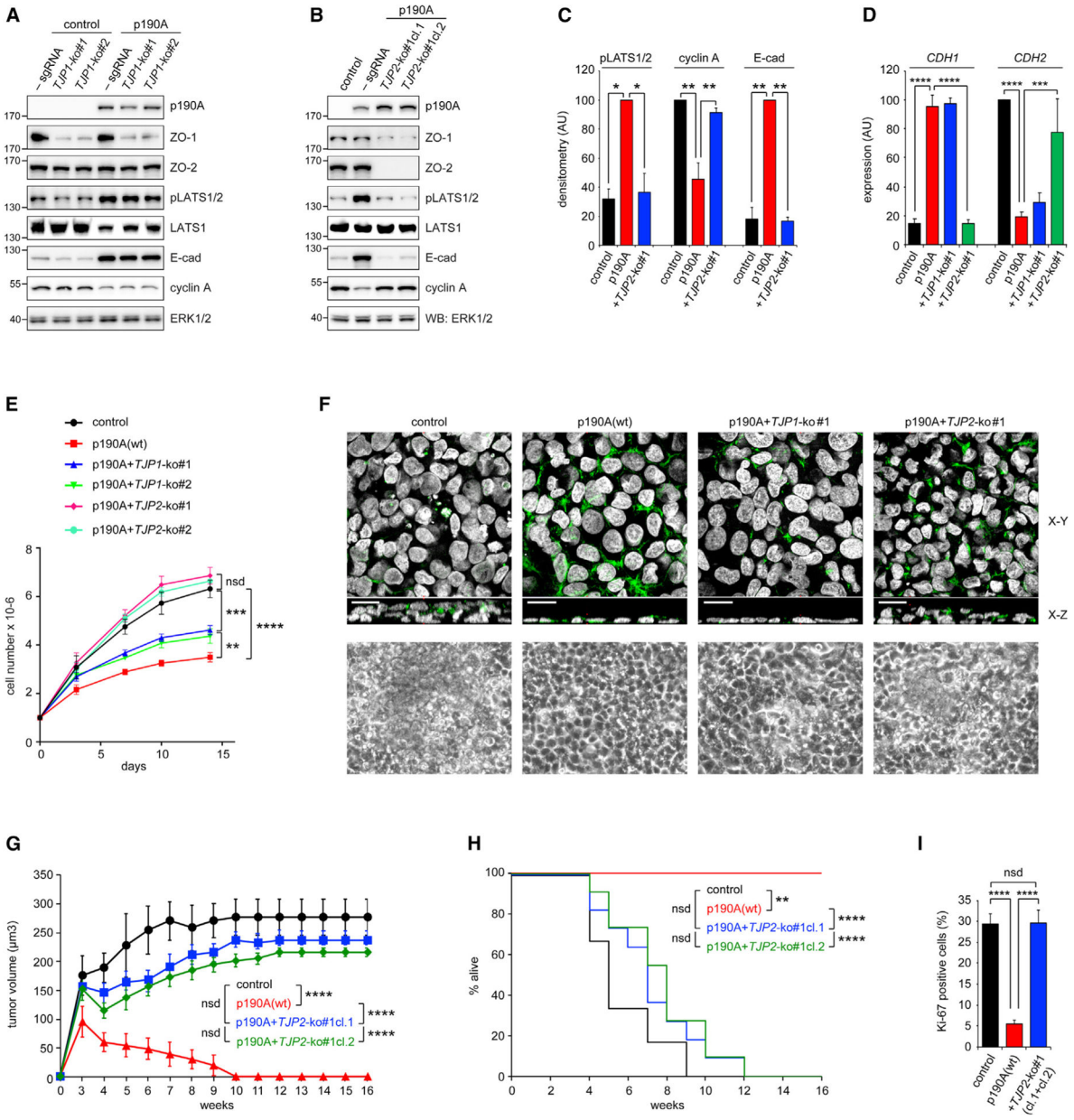

Figure 4. ZO-2 is necessary for p190A to activate LATS1 kinase, promote CIP, elicit MET, and suppress tumorigenesis of H661 cells in nude mice

(A) Western blots of whole-cell lysates to detect p190A, ZO-1, ZO-2, pLATS1/2, LATS, E-cadherin, cyclin A, and ERK1/2 in control cells and H661-p190A cells ± *TJP1*-KO.

(B) Western blots of whole-cell lysates to detect p190A, ZO-1, ZO-2, pLATS1, E-cadherin, cyclin A, and ERK1/2 in control cells and H661-p190A cells ± *TJP2-KO*. For this experiment, two single cell clones, cl.1 and cl.2 with undetectable ZO-2, were successfully isolated from a pooled population of cells expressing *TJP2* sgRNA#1.

(C) Quantification by densitometry of pLATS1/2, cyclin A, and E-cadherin levels detected by western blotting as shown in (B). Data are presented as mean ± SD (n = 3). Statistical testing was performed using pairwise Student's t test as indicated by brackets.

(D) Transcript levels for *CDH1* and *CDH2*, as determined by qPCR. Data are presented as mean ± SD (n = 6). Statistical testing was performed using pairwise Student's t test as indicated by brackets.

(E) Growth curves for control and H661-p190A cells with or without KO of *TJP1* or *TJP2*. 1 × 10^6 cells were seeded per well of a 6-well plate in triplicate and propagated for the number of days indicated with a change of medium every 2 days. Cell number was quantified manually. Data are presented as mean ± SD. Statistical testing was performed by pairwise Student's t test as indicated by brackets.

(F) *TJP2* is necessary for p190A to restore monolayer architecture. Top panels show confocal microscopy of control cells as well as H661 cells with expression of p190A ± *TJP1* or ± *TJP2* KO. Cells are labeled with fluorescent phalloidin (green) and the DNA-binding dye DRAQ5 (white). Scale bars represent 10 μm. Bottom panels show phase images for the same conditions.

(G) Cumulative xenograft tumor volume in mice injected with control cells (n = 6) or H661-p190A (n = 7), as well as two clones of H661-p190A cell with CRISPR-Cas9-mediated KO of *TJP2* (n = 11 each). Data are presented as mean ± SEM. Statistical testing was performed using pairwise Student's t test as indicated by brackets. Data are presented as mean ± SEM.

(H) Kaplan-Meier survival plot for the cohort of mice described in (G). Statistical testing was performed using pairwise log-rank test as indicated by brackets.

(I) Quantification of immunohistochemistry to detect Ki-67-positive cells in tumors 3 weeks after injection of control cells or H661-p190A cells ± *TJP2-KO*. Data are presented as mean ± SEM with n = 5 mice and >600 nuclei scored per condition. Statistical testing was performed using pairwise Student's t test as indicated by brackets.

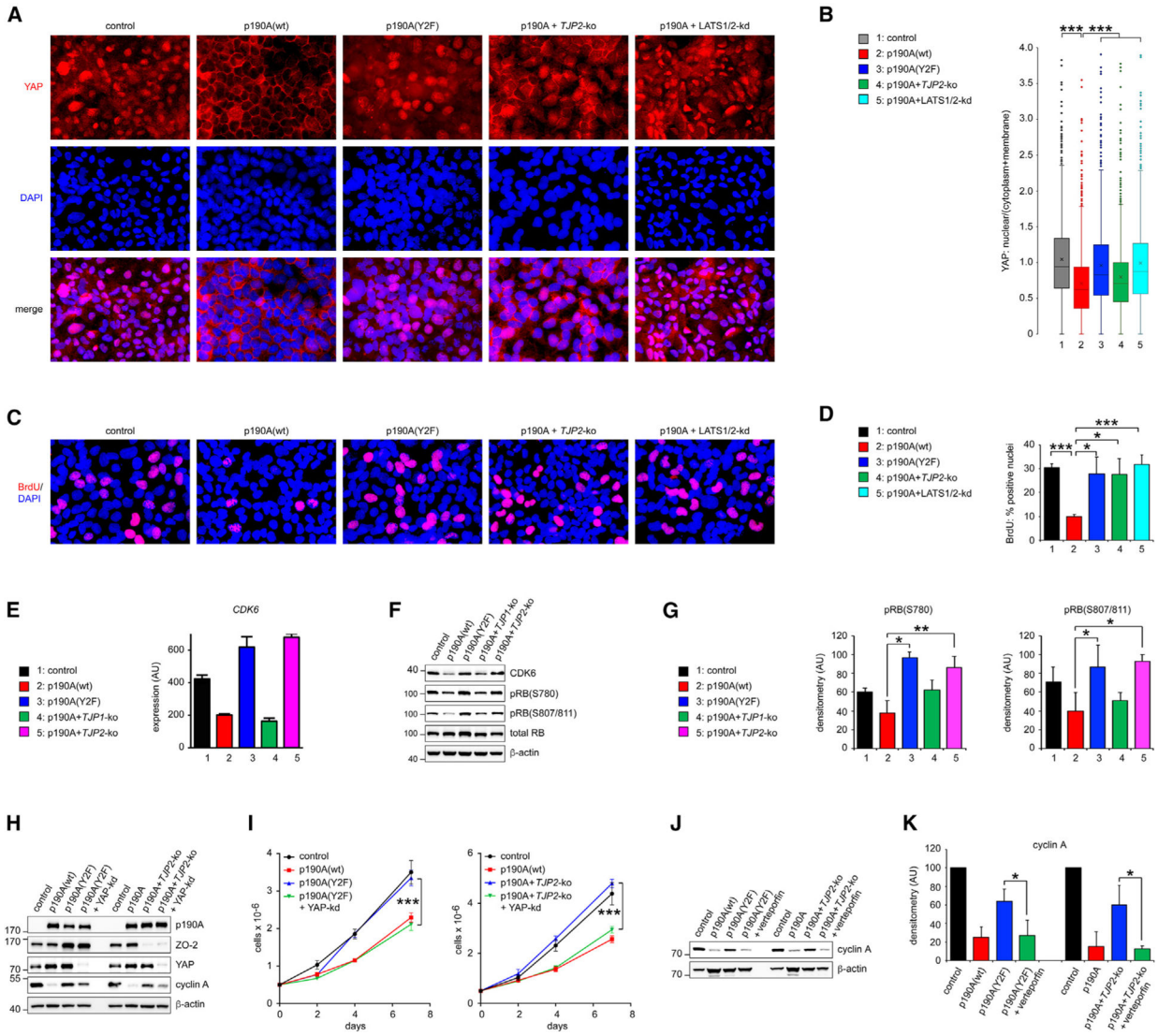

Figure 5. RasGAP interaction and ZO-2 are essential to p190A-mediated modulation of YAP function and cell-cycle regulation

(A) Immunofluorescence to detect YAP protein (red) in H661 cells with or without expression of p190A(WT) or p190A(Y2F), as well as in H661-p190A cells with KO of *TJP2* or depleted of LATS1/2. Nuclei were labeled with DAPI (blue).

(B) Quantification using CellProfiler (github.com) of nuclear/cytoplasmic YAP from the experiment illustrated in (A). The experiment was performed with three biological replicates and a minimum of 912 cells sampled from each condition. Data are presented as mean ± SEM. Statistical testing was performed using pairwise Student's t test as indicated by brackets.

(C) Immunofluorescence to detect BrdU-positive nuclei in H661 cells with or without expression of p190A(WT) or p190A(Y2F), as well as in H661-p190A cells with KO of *TJP2* or depleted of LATS1/2. Nuclei were labeled with DAPI (blue).

(D) Quantification using CellProfiler (github.com) of BrdU-positive nuclei from the experiment illustrated in (C). The experiment was performed with three biological replicates

and a minimum of 626 cells sampled from each condition. Data are presented as mean ± SD (n = 3). Statistical testing was performed using pairwise Student's t test as indicated by brackets.

(E) CDK6 transcript levels in H661 cells with or without expression of p190A(WT) or p190A(Y2F), as well as in H661-p190A cells with KO of *TJP1* or *TJP2*.

(F) Western blotting to detect CDK6, pRB(S780), pRB(S807/811), total RB, and β-actin in whole-cell lysates from H661 cells with or without expression of p190A(WT) or p190A(Y2F), as well as in H661-p190A cells with KO of *TJP1* or *TJP2*.

(G) Quantification of pRB(S780) and pRB(S807/811) levels by densitometry of western blots as shown in (F). Data are presented as mean ± SD. Statistical testing was performed using pairwise Student's t test as indicated by brackets (n = 3).

(H) Western blotting to detect p190A, ZO-2, YAP, cyclin A, and β-actin in whole-cell lysates from H661 cells with or without expression of p190A(WT) or p190A(Y2F) ± YAP-KD, as well as in H661-p190A cells with KO of *TJP2* ± YAP-KD.

(I) Growth curves for control and H661 cells reconstituted with p190A(WT) or p190A(Y2F) ± YAP-KD, as well as in H661-p190A cells with KO of *TJP2* ± YAP-KD. 5×10^5 cells were seeded per well of a 6-well plate in triplicate and propagated for the number of days indicated with a change of medium every 2 days. Cell number was quantified manually. Data are presented as mean ± SD (n = 3). Statistical testing was performed using pairwise Student's t test as indicated by brackets.

(J) Western blotting to detect cyclin A and β-actin in whole-cell lysates from H661 cells with or without expression of p190A(WT) or p190A(Y2F) ± verteporfin, as well as in H661-p190A cells with KO of *TJP2* ± verteporfin. Cells were treated with 3 μM verteporfin for 48 h at 37°C.

(K) Quantification of cyclin A levels by densitometry of western blots as shown in (J). Data are presented as mean ± SD. Statistical testing was performed using pairwise Student's t test as indicated by brackets (n = 3).

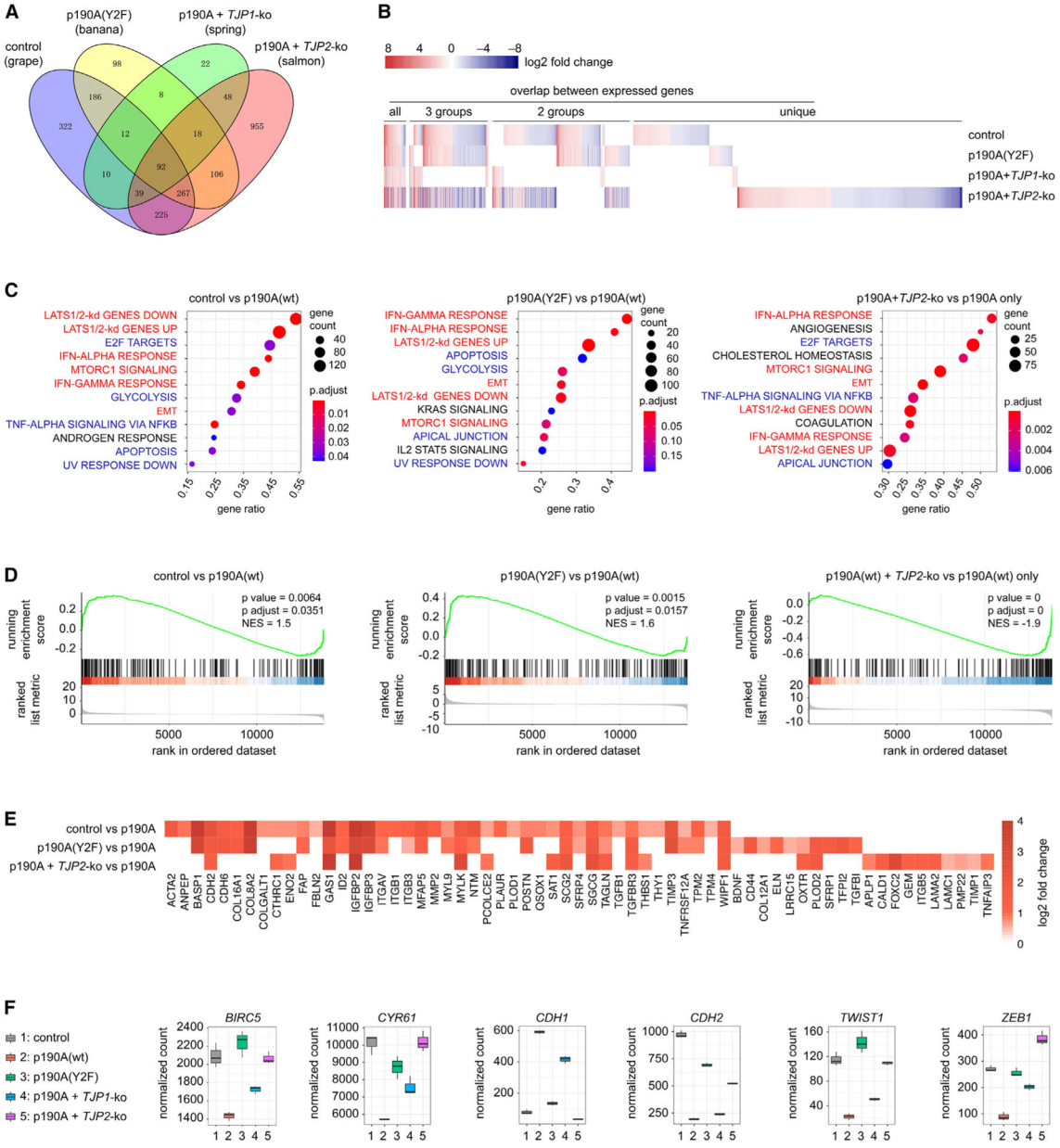

Figure 6. RasGAP and ZO-2 are required for transcriptomic alterations elicited by p190A

(A) Venn diagram of differentially expressed genes (DEGs) as determined by RNA sequencing in H661-p190A(WT) cells relative to control cells, or H661-p190A(WT) cells ± *TJP1* or ± *TJP2* KO, as well as cells expressing p190A(Y2F). The threshold for differential expression was set at basemean ≥20 and $\log_2$(fold change) ≥1 or ≤ −1with an adjusted p value of <0.05. All experimental conditions were performed in triplicate.

(B) Heatmap displaying $\log_2$(fold change) of DEGs from control, p190(Y2F), 190A(WT) + *TJP1*-KO, and 190A(WT) + *TJP2*-KO cells compared to H661-p190A(WT) cells. DEGs that were common among all four, three, or two conditions, or found in a single condition only when compared to p190A(WT), are shown. Relative to p190A(WT), upregulated genes are

shown in red, downregulated genes are shown in blue, and genes not significantly changed are shown in white. Darker color intensity indicates greater fold change.
(C) Dot plots showing the results of GSEA for the 12 most enriched gene sets in pairwise comparisons of DEGs in H661-p190A(WT) cells relative to control cells, or H661-p190A(WT) cells relative to p190A(Y2F) cells, or H661-p190A(WT) cells with or without KO of *TJP2*. Fifty hallmark gene sets from MSigdb and two customized Hippo signaling gene sets were included for the GSEA analysis. We defined the LATS1/2-KD UP/DOWN gene sets from DEGs of LATS1/2 depletion in H661-p190A expression cells, with the threshold set at basemean >100, $\log_2$(fold change) ≥1 or ≤ −1, and adjusted p value ≤0.001. We then defined the 343 most upregulated genes as LATS1/2-KD UP gene set and 239 most downregulated genes as LATS1/2-KD DN gene set. Red color indicates signaling pathways regulated by all three conditions, blue color highlights signaling pathways regulated by two conditions, and black color represents signaling pathways restricted to the specific condition.
(D) Waterfall plots of GSEA EMT gene sets in H661-p190A(WT) relative to control cells, H661-p190A(WT) relative to p190A(Y2F) cells, or H661-p190A(WT) cells ± *TJP2* KO.
(E) Heatmap of leading-edge genes that account for the enrichment of EMT gene sets. Red color makes positively regulated transcripts for each condition. The darker the color, the greater the fold difference. Leading-edge genes shared among the three conditions are *CDH2*, *GAS1*, *IGFBP3*, *MYLK*, *SCG2*, *SGCG*, *TAGLN*, *TGFBR3*, and *WIPF1*.
(F) Expression of the key Hippo genes, *BIRC5* and *CYR61*, and EMT genes, *CDH1*, *CDH2*, *TWIST1*, and *ZEB1*, as determined by RNA sequencing for the following conditions: control, H661-p190A(WT), and p190A(Y2F), as well as H661-p190A(WT) with *TJP1* or *TJP2* KO.

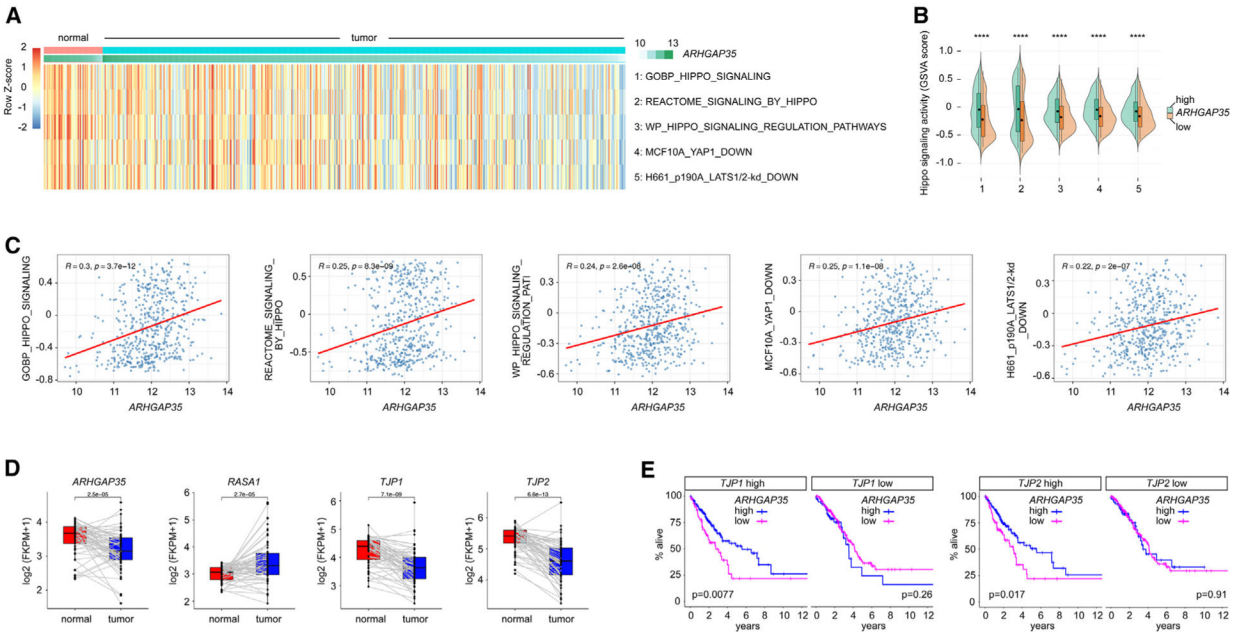

Figure 7. Low *ARHGAP35* expression is associated with reduced lifespan in patients with high, but not low, levels of TJP1/2 transcripts

(A) Heatmap of activity scores of Hippo pathways with data normalized from −2 (blue) to +2 (red) in 524 LUAD samples and 59 uninvolved (normal tissue) samples retrieved from TCGA. By using GSVA raw counts, data were used for analyzing Hippo pathway activity using the four gene sets from MSigDB (GOBP_HIPPO_SIGNALING, REACTOME_SIGNALING_BY_HIPPO, WP_HIPPO_SIGNALING_REGULATION_PATHWAYS, and MCF10A_YAP1_DOWN) and one customized H661_p190A_LATS1/2 kd_DOWN gene set, which was defined as previously described. Expression levels of *ARHGAP35* ranging between 10 and 13 are presented as variance-stabilizing transformation (VST) transformed data calculated by DESeq2. Higher pathway activities are shown in red, while lower pathway activities are shown in blue. Original GSVA scores were scaled and shown as *Z* scores between −2 and +2.

(B) LUAD patients were divided into two groups with the median of p190A expression set as cutoff. Next, Hippo signaling activity of GSVA scores were compared between these two groups using Student's t test.

(C) Correlation between *ARHGAP35* expression (VST transformed data by DESeq2) and Hippo signaling (GSVA scores) in 524 LUAD solid tissue samples tested by Pearson correlation analysis.

(D) Differences in *ARHGAP35*, *RASA1*, *TJP1*, and *TJP2* transcript levels in 59 pairs of matched normal and tumor tissue from patients with LUAD.

(E) Survival of patients with high and low *ARHGAP35* expression stratified according to high versus low transcript levels of *TJP1* or *TJP2*. Survival data from a total of 484 patients were available for this analysis. Sixteen patients with detectable *ARHGAP35* mutation information were excluded from this analysis. Medium value was used as cutoff for separating *ARHGAP35*, *TJP1*, or *TJP2* high- and low-expression groups.

KEY RESOURCES TABLE

REAGENT or RESOURCE	SOURCE
Antibodies	
β-actin	Invitroge
Cdk6	Cell Sign Technolo
Cyclin A	Santa Cru Biotechn
E-Cadherin	BD Biosc
ERK1	Santa Cru Biotechn
ERK1/2	Millipore
FLAG-M2	Millipore
GFP	Santa Cru Biotechn
Ki-67	Thermo F Scientific
phospho-LATS1/2(S909/S872)	Cell Sign Technolo
LATS	Cell Sign Technolo
N-cadherin	Cell Sign Technolo
MEK	Cell Sign Technolo
pMEK	Cell Sign Technolo
p190A	BD Biosc
p190B	BD Biosc
Rb	Cell Sign Technolo
phospho-RB(S780)	Cell Sign Technolo
phospho-RB(S807/S811)	Cell Sign Technolo
YAP1	Cell Sign Technolo
phospho-YAP1(S127)	Cell Sign Technolo
ZO-1	Cell Sign Technolo
ZO-1	Cell Sign Technolo
ZO-1	Proteinte
ZO-2	Cell Sign Technolo

REAGENT or RESOURCE	SOURCE
ZO-2	Proteinte
ZO-2	Boster
goat anti-mouse/Alexa 555	Invitroge
goat anti-rabbit/Alexa 488	Invitroge
goat anti-mouse/HRP	Jackson ImmunoR
goat anti-rabbit/HRP	Jackson ImmunoR
Bacterial and virus strains	
DH5-alpha (High Efficiency)	New Eng Biolabs
Chemicals, peptides, and recombinant proteins	
Fugene6	Promega
Polybrene	Santa Cru Biotechn
Phalloidin/Alexa 488	Invitroge
Phalloidin/Alexa 594	Invitroge
Verteporfin	Beijing Biosynth Biotechn Co.
Critical commercial assays	
Click-iT™ EdU Pacific Blue™ kit	Invitroge
iScript cDNA synthesis kit	BioRad
Luna Universal qPCR Master Mix	New Eng Biolabs
RNeasy Mini Kit	Qiagen
Deposited data	
RNA sequencing data	This pape
Experimental models: Cell lines	
NCI-H661	ATCC
NCI-H226	ATCC
NCI-H2087	ATCC
MDA-MB-231	ATCC
MDCK w. ZO-1-KD w. EGFP only	Jerrold R laboratory
MDCK w. ZO-1-KD w. EGFP-ZO-1 (WT) (knockdown-resistant)	Jerrold R laboratory
MDCK w. ZO-1-KD w. EGFP	Jerrold R laboratory
MDCK w. ZO-1-KD w. EGFP-ZO-1(DPDZ1) (knockdown-resistant)	Jerrold R laboratory
MDCK w. ZO-1-KD w. EGFP-ZO-1(DU5GuK) (knockdown-resistant)	Jerrold R laboratory
MDCK w. ZO-1-KD w. EGFP-ZO-1(DABR) (knockdown-resistant)	Jerrold R laboratory

REAGENT or RESOURCE	SOURCE
MDCK w. ZO-2-KD w. EGFP (knockdown-resistant)	Jerrold R laboratory
MDCK w. ZO-2-KD w. EGFP-ZO-2 (knockdown-resistant)	Jerrold R laboratory
Experimental models: Organisms/strains	
Mouse: nude Foxn1nu/Foxn1nu	The Jacks Laborator
Oligonucleotides	
See Table S3 for Oligonucleotides sequences	N/A
Recombinant DNA	
Plasmid: pUltra-hot-myc-p190A(WT)	This pape
Plasmid: pUltra-hot-myc-p190A(Y2F)	This pape
Plasmid: pLv5-Cas9-Neo	Millipore
Plasmid: FgH1tUTG	Addgene
Plasmid: FgH1tUTG w. sgRNA	This pape
Plasmid: *TJP2sgRNA* in pLentiGuide-Puro	Addgene
Plasmid: pLXV-EF1a-IRES-Puro	Addgene
Plasmid: pLXV-EF1a-ZO-2-FLAG IRES-Puro	This pape
Plasmid: pLXV-EF1a-GFP-FLAG IRES-Puro	This pape
Plasmid: pZIP encoding *ARHGAP35* shRNA #1 5′-TGCTGTTGACAGTGAGCGCCCTAATCTAGATGAAATAGAATAGTGAAGCCACAGATGTATTCTATTTCATCTAGATTAGGTTGCCTACTGCCTCGGA-3	transOMI Technolo
Plasmid: pZIP encoding *ARHGAP35* shRNA #2 5′-TGCTGTTGACAGTGAGCGCAAGTAGGGAACAGCTAACTGATAGTGAAGCCACAGATGTATCAGTTAGCTGTTCCCTACTTATGCCTACTGCCTCGGA-3′	transOMI Technolo
Plasmid: pLV[shRNA]-Puro-U6>{shYAP553} shRNA 5′-GGTCAGAGATACTTCTTAAATCTCGAGATTTAAGAAGTATCTCTGACC-3′	VectorBu
Software and algorithms	
Adobe Photoshop versions CC2018-2021; RRID: SCR_014199	Adobe
Adobe Illustrator version CC2020-2021; RRID: SCR_010279	Adobe
R version 3.63	R Core T
RStudio	R Core T